Recent progress in multi-wavelength fiber lasers: principles, status, and challenges

Hualong Chen (陈华龙)[1,†], Xiantao Jiang (蒋先涛)[1,2,†], Shixiang Xu (徐世祥)[1,*], and Han Zhang (张 晗)[1,]**

[1]*SZU-NUS Collaborative Innovation Center for Optoelectronic Science & Technology, Collaborative Laboratory of 2D Materials for Optoelectronic Science and Technology of Ministry of Education, College of Physics and Optoelectronic Engineering, Shenzhen University, Shenzhen 518060, China*

[2]*College of Chemistry and Environmental Engineering, Shenzhen University, Shenzhen 518060, China*

**Corresponding author: hzhang@szu.edu.cn; **corresponding author: shxxu@szu.edu.cn*

Received October 28, 2019; accepted March 1, 2020; posted online April 14, 2020

In recent years, multi-wavelength fiber lasers play a significant role in plenty of fields, ranging from optical communications to mechanical processing and laser biomedicine, owing to their high beam quality, low cost, and excellent heat dissipation properties. Benefitting from increasing maturity of optical elements, the multi-wavelength fiber laser has made rapid developments. In this review, we summarize and analyze diverse implementation methods covering continuous wave and pulsed fiber lasers at room temperature conditions: inserting an optical filter device and intensity-dependent loss structure in the resonant cavity, and applying ultrafast nonlinear optical response of materials and a dual-cavity structure. Finally, future challenges and perspectives of the multi-wavelength fiber laser are discussed and addressed.

Keywords: multi-wavelength fiber laser; optical filter; nonlinear polarization rotation; nonlinear amplification loop mirror; 2D materials.

doi: 10.3788/COL202018.041405.

1. INTRODUCTION

Nowadays, the fiber laser has attracted much attention due to its enormous superiorities such as admirable beam quality, cheapness, good compatibility, and simple and compact structure[1–6]. With the popularity of computers and mobile phones, people put forward higher requirements for optical communication systems. To unlock the available fiber communication capacity and improve for a higher communication rate, the dense wavelength division multiplexing (DWDM) technique has been intensively adopted and investigated[7–9]. The DWDM system needs multiple laser sources or a laser source launching multiple wavelengths, and the implementation of multi-wavelength laser doubtlessly saves in cost to a large extent. On the other hand, the multi-wavelength fiber laser (MWFL) can be naturally integrated into the optical fiber communication system. Hence, MWFLs are very attractive as ideal light sources for a DWDM fiber communication system[10,11]. In addition, MWFLs can be applied to fiber sensors[12], spectroscopy[13], phased array antennas[14], dual-wavelength combs[15], and microwave generation[16], as shown in Fig. 1. Consequently, MWFLs have become a research hotspot and caused enormous interest and attention in the world.

For MWFLs, when the spacing between the neighbor wavelengths is less than the uniform linewidth of the gain fiber, the intense mode competition and mode hopping, existing in a homogeneously broadening gain medium, are inevitable and serious. The homogeneous gain broadening is the key factor for suppressing the multi-wavelength operation whenever pulsed or continuous wave (CW) operation forms. Accordingly, to obtain stable MWFLs, it is necessary to weaken the homogeneous broadening effect of the gain fiber to restrain mode competition and mode hopping[17–19]. To solve these problems, researchers cooled the erbium-doped fiber with liquid nitrogen, and the homogeneous broadening effect is enormously suppressed[20,21]. However, the method has some disadvantages in practical applications such as high cost and complex and incompact structure.

In the room temperature condition, there are a few methods to obtain multi-wavelength operation: using the frequency shift feedback technique[22–24], directly inserting filter devices[25–30], adding wavelength or intensity-dependent loss structures[31,32], and the high nonlinear effect of materials[33,34]. All of the methods mentioned above are aiming to weaken the homogeneous broadening effect to obtain multi-wavelength operation.

In the MWFLs, there are two main categories: CW[35–40] and pulsed sources[41–47]. For multi-wavelength CW fiber lasers, the cavity must have a multi-wavelength generator. However, compared with the multi-wavelength CW fiber laser, the multi-wavelength pulsed fiber laser must simultaneously possess a pulse laser transverter [e.g., saturable absorber (SA) and electro-optic modulator] and a multi-wavelength generator. The SA supplies nonlinear absorption for lasers and transforms the CW laser into pulsed operation. The SA device and multi-wavelength generator work together[48] and realize multi-wavelength pulsed laser operation.

What the MWFL discussed above possesses is a single-gain medium in the cavity, which owns a limited gain

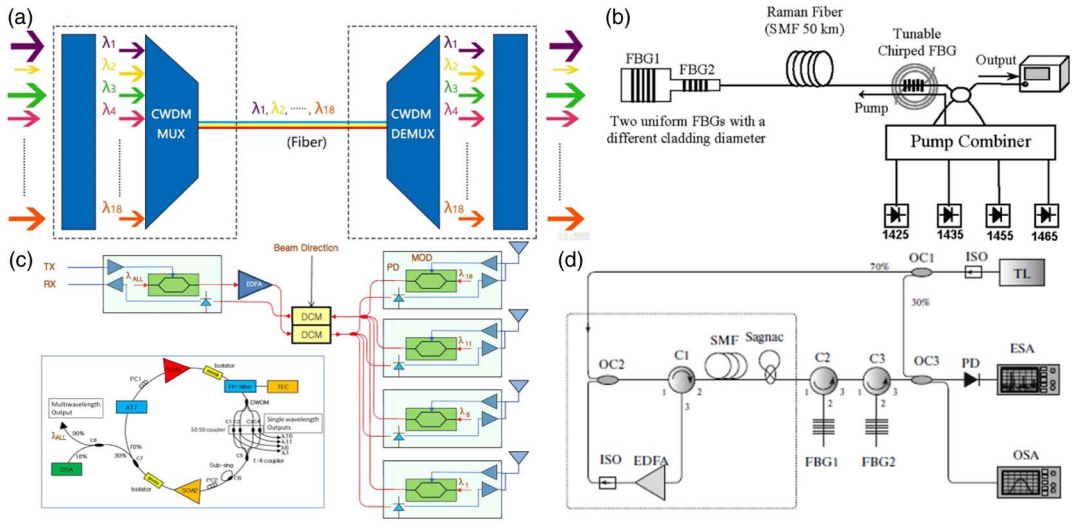

Fig. 1. Applications of MWFL: (a) DWDM technology for an optical communication system, and (b) the multi-wavelength Raman fiber laser for long-distance simultaneous measurement of strain and temperature selected from Ref. [12]. (c) Phased array antenna system selected from Ref. [14]. (d) Microwave signal generation based on a multi-wavelength Brillouin fiber laser selected from Ref. [16].

spectrum. The single-gain medium fiber laser cannot obtain wide range multi-wavelength operation. We also summarize dual-cavity pulsed fiber lasers owning two gain media, naturally generating two colors, and the two beams independently operate. Dual-wavelength pulsed fiber lasers with broad wavelength range separation are applied in many fields such as nonlinear frequency conversion, the pump–probe technique, chemical sensing, and Raman scattering spectra.

Here, we briefly review the current status of the MWFL, especially passively mode-locked multi-wavelength operation fiber lasers, and then analyze and discuss the principle, challenges, and perspectives of MWFLs.

2. MULTI-WAVELENGTH CONTINUOUS WAVE FIBER LASERS

The multi-wavelength CW fiber laser has attracted the attention of many researchers due to its huge potential in application fields such as optical fiber sensors, millimeter-wave generators, and optical communications systems[35,49–51]. For multi-wavelength CW fiber lasers, there are two main categories according to operating principles: active modulation (e.g., frequency shifter) and passive modulation (e.g., filter structures and intensity-dependent loss structures).

A. Multi-Wavelength CW Fiber Laser with the Aid of a Frequency Shifter

By introducing a frequency shifter into the cavity, the optical signal circulates and passes through the frequency shifter to produce the frequency shift[23]. Therefore, one wavelength cannot be continuously amplified on account of frequency shift. As a result, the uniform broadening of gain fiber is suppressed to a great extent, and the frequency shifter prevents the emission from a single wavelength and results in stable MWFL operation at room temperature conditions. Zhou *et al.* reported a multi-wavelength Er-doped fiber laser (EDFL) with the aid of sinusoidal phase modulation feedback (see Fig. 2)[24]. The function of the phase modulator was demonstrated by a contrast experiment [see Figs. 2(b) and 2(c)].

B. Multi-Wavelength CW Fiber Laser with the Aid of Filter Structures

Active modulator techniques need electrical devices driven by external power, which increases insertion loss

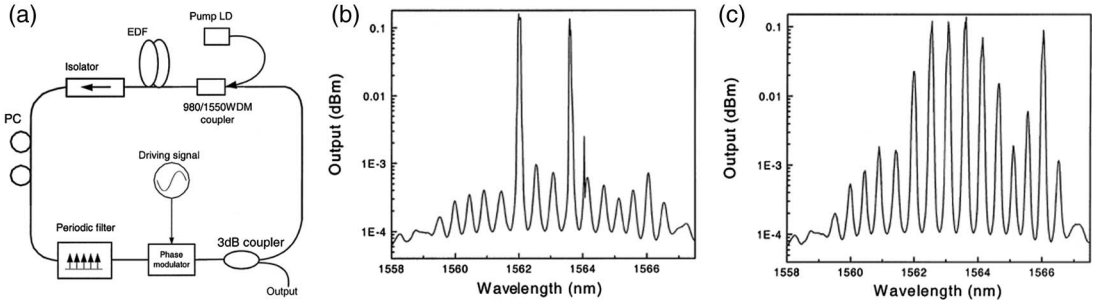

Fig. 2. Multi-wavelength EDFL based on a phase modulator: (a) the schematic of the experimental setup; the output spectrum characteristics (b) without modulation feedback and (c) with modulation feedback. Selected from Ref. [24].

and breaks all-fiber structures. Therefore, the multi-wavelength CW fiber laser based on passive modulation structures has been intensively exploited by researchers around the world. In the multi-wavelength CW fiber laser, an ultra-narrow linewidth mode selecting filter is indispensable[52]. Filter devices pick up designated wavelengths from the net gain spectrum of the fiber laser and effectively suppress homogeneous gain broadening to produce multiple wavelengths in the fiber laser. There are several passive modulation structures utilized to achieve multi-wavelength operation such as the comb filter, Mach–Zehnder interferometer (MZI)[26–28,53–56], single-mode fiber (SMF)–multi-mode fiber (MMF)–SMF (SMS) interferometer[57,58], band-pass filter, and chirped fiber Bragg grating (CFBG)[17,59–62].

MZI generally is composed of two optical couplers (OCs). The first OC divides light equally into two parts, which interfere with each other in the second OC. Two beams experience different paths with a tunable phase shift to generate the comb filter effect. Luo *et al.* demonstrated multi-wavelength CW operation in an EDFL with the help of the dual-pass MZI filter[27]. The tunable transmission spectra of the MZI comb filter, resulting in multi-wavelength operation, were accurately measured. The spacing and the position of transmission spectral peaks were changed by only adjusting the polarization controller (PC), as shown in Fig. 3(b), while 14-wavelength and 29-wavelength operations were obtained by finely adjusting the PC in different proper positions, respectively. However, they could not achieve multi-wavelength mode-locked operation for lack of a mode locker device in the cavity.

The SMS structures also generate the comb filter effect based on the multi-mode interference (MMI) effect based on the theory of generating multi-wavelength operation as the MZI, which means the MWFL can be produced with the aid of the SMS interferometer.

Zhang *et al.* demonstrated stable tri-wavelengths in a Tm-doped fiber laser (TDFL) by utilizing the SMS interferometer[57]. The MMI effect is generated in the MMF, which excites all the modes. However, similarly, they only realized multi-wavelength CW operation for lack of a mode locker. Anum *et al.* reported a compact tunable and switchable single/dual-wavelength EDFL based on the SMS structure, and then carefully adjusted the PC position of the paddle (see Fig. 4). The dual-wavelength laser, operating at 1558.15 and 1565.38 nm, was finally obtained with a small power fluctuation and wavelength drift[30]. Recently, Yang *et al.* experimentally realized a stable mode-locked pulse fiber laser based on the SMS structure alone with a pulse width of 528 fs and repetition rate of 14.34 MHz[63]. However, the multi-wavelength mode-locked fiber-laser-based SMS interferometer has not been reported.

A fiber grating (FG) has been intensively applied in MWFL and fiber sensors due to their wavelength-pick nature, which has the unique advantage of fiber

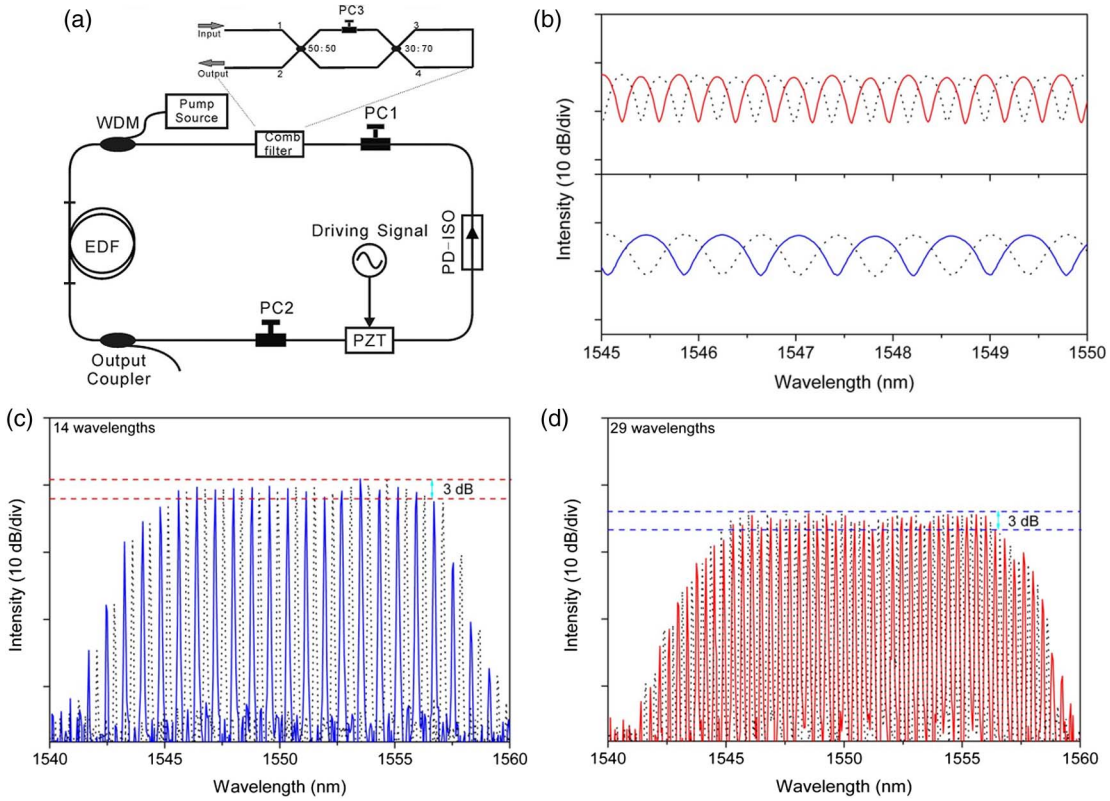

Fig. 3. Multi-wavelength operation based on the MZI filter effect: (a) the experimental schematic of an EDFL; (b) the comb filter transmission spectra; (c) the spectral characteristics of 14-wavelengths operation; (d) the spectral characteristics of 29-wavelengths operation. Selected from Ref. [27].

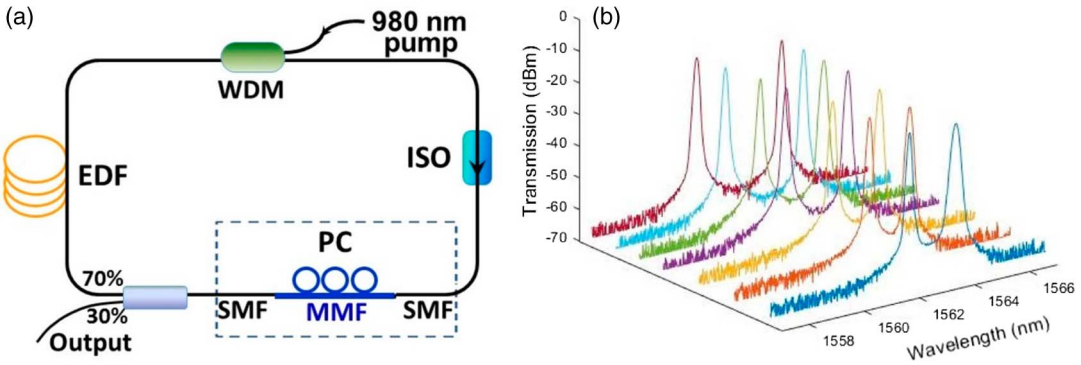

Fig. 4. MWFL based on the SMS interferometer: (a) the experimental schematic diagram of dual-wavelength EDFL; (b) the output spectral tunable dual-wavelength fiber laser. Selected from Ref. [30].

compatibility. There are various FGs, such as a CFBG[53,64–67], polarization-maintaining long-period FG (PM-LPFG)[68], few-mode FG (FMFG)[69,70], and MMF Bragg grating (MFBG)[71]. CFBG generally has a narrow-band reflection spectrum and possesses a natural wavelength picking characteristic. Two FBGs, combining a Fabry–Perot (F-P) filter, have a relatively complex reflection spectrum.

He *et al.* reported a dual-wavelength narrow linewidth single-longitudinal mode (SLM) operation linear-cavity EDFL by applying an FBG-based F-P filter and a narrow-band FBG. Finally, three different cases of tunable dual-wavelength fiber lasers, emitting at 1569.38 and 1569.60 nm, 1568.84 and 1569.38 nm, and 1569.61 and 1569.81 nm, were obtained. Wang *et al.* demonstrated a dual-wavelength TDFL with the aid of three FBGs, as shown in Figs. 5(a)–5(c), which are from two linear resonant cavities, and the central wavelengths are 1942 and 2020 nm, respectively[66].

These filter devices are made from fiber and thus assures the all-fiber laser structure, which is good for stable multi-wavelength operation. More interestingly, the spacing and the position of the transmission spectral peak can be altered by adjusting an appropriate position of the PC, and a tunable MWFL was intensively explored.

In addition, the MWFL also can be obtained based on two types of filter combinations. For instance, Zhao *et al.* demonstrated a switchable MWFL with the aid of a combined filter that is assembled with a phase-shifted fiber Bragg grating (PSFBG) and an MZI[72]. The four stable output cases, single-, dual-, triple-, and quadruple-wavelength emissions, can be realized, as shown in Figs. 5(d) and 5(e).

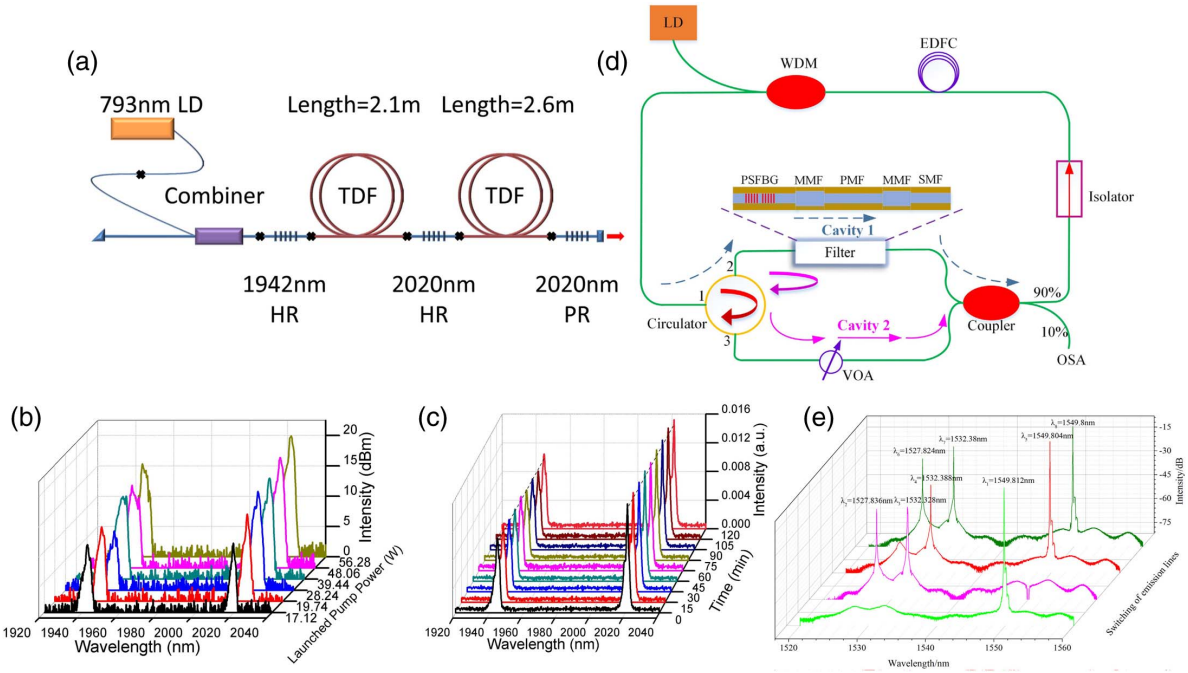

Fig. 5. Multi-wavelength fiber laser and the output characteristics: (a) the schematic diagram of dual-wavelength EDFL; (b) optical spectral evolution with different pump power; (c) the stability measurement of optical spectra. Selected from Ref. [66]. (d) The schematic diagram of multi-wavelength TDFL; (e) the stable tri-wavelength operation. Selected from Ref. [72].

C. Multi-Wavelength CW Fiber Laser Based on Intensity-Dependent Loss Structures

There is another way to achieve a multi-wavelength by applying an intensity-dependent loss structure, including nonlinear polarization rotation (NPR)[73,74] and a nonlinear amplification loop mirror (NALM)[75–77]. The two structures transform effective gain broadening of doped rare earth gain fiber from homogeneous to inhomogeneous and suppress the strong longitudinal mode competition and hopping, which provide the possibility for multi-wavelength operation in a fiber laser.

The NPR structure includes a polarization-dependent isolator (PD-ISO) and two PCs. The experimental setup, as shown in Fig. 6(a), is so simple and compact, which saves cost and achieves an all-fiber structure[78].

Yan *et al.* presented the transmission equation for the NPR structure and the birefringent fiber, as shown in Fig. 6(b). The transmission rule of the setup was expressed by

$$T = \cos^2\theta_1 \cos^2\theta_2 + \sin^2\theta_1 \sin^2\theta_2 + \frac{1}{2}\sin(2\theta_1)\sin(2\theta_2)\cos\left(\Delta\varphi_L + \Delta\varphi_{\mathrm{NL}}\right). \quad (1)$$

In the schematic diagram, θ_1 is the angle between the fast axis of the birefringent fiber and the polarization direction of the laser, and θ_2 is the angle between the fast axis of the birefringent fiber and the orientation of the polarizers, as shown in Fig. 6(b). $\Delta\varphi_L$ and $\Delta\varphi_{\mathrm{NL}}$ are the linear and nonlinear phase delay, respectively, which can be expressed as follows:

$$\Delta\varphi_N = 2\pi L B_m/\lambda, \quad (2)$$

$$\Delta\varphi_{\mathrm{NL}} = 2\pi n_2 P L \cos(2\theta_1)/\lambda A_{\mathrm{eff}}, \quad (3)$$

where n_2 is the nonlinear refractive index, P is the light power, L is the length of birefringent fiber, $B_m = |n_x - n_y|$ is the birefringence of fiber, λ is the transmitting wavelength in the cavity, and A_{eff} is the effective mode area[78].

The transmission equation is a sinusoidal fashion. The transmittance (also meaning loss) of the setup changes with phase delay introduced by the PC and the light intensity. As is well known, the NPR structure can achieve mode-locked operation due to the light transmittance increasing as the light intensity increases. However, if we make the setup transmittance at the state where transmittance decreases with light intensity, the setup can act as a kind of light intensity balancer. The balanced effect can effectively restrain the uniform broadening effect of doped

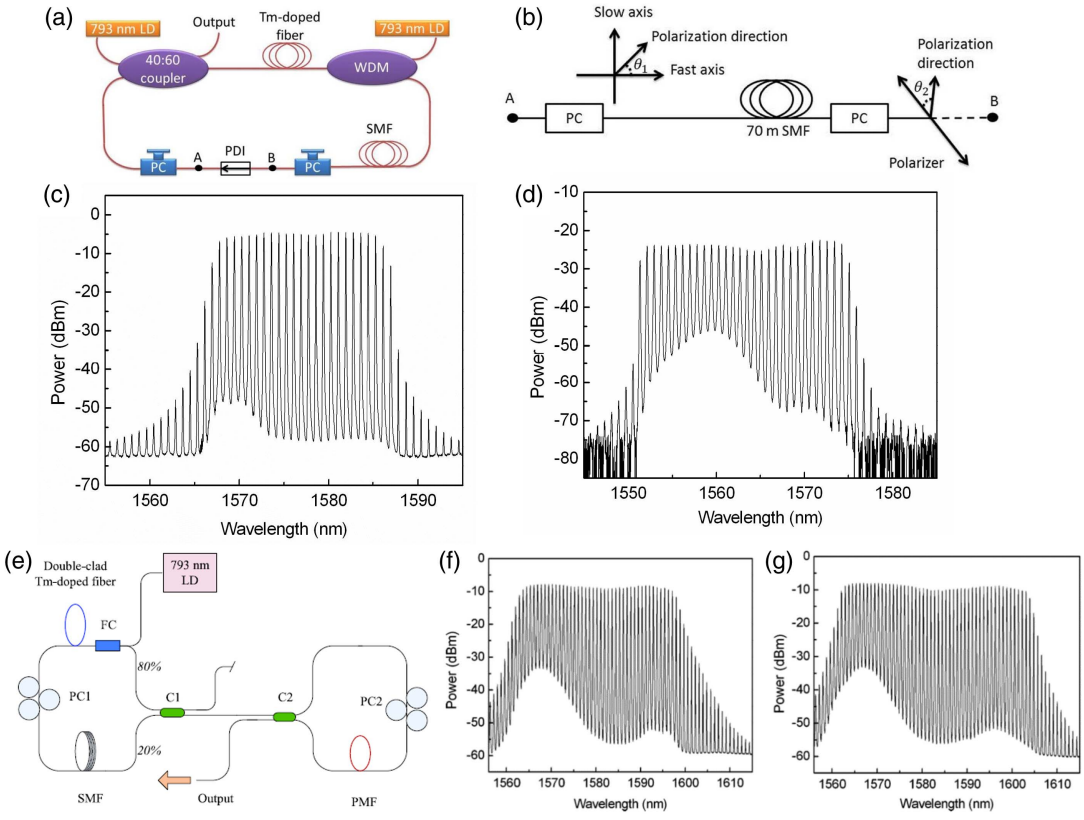

Fig. 6. MWFL based on two types of intensity-dependent loss structures: (a) schematic of the NPR mode-locked TDFL; (b) working principle of the NPR structure. Selected from Ref. [78]. Two cases of output spectrum of MWFL based on NPR structures: (c) 22-wavelength operation; (d) 28-wavelength operation. Selected from Ref. [73]. (e) The experimental setup of the NALM structure. Output spectrum characteristics of EDFL based on the NALM structure at two different states by adjusting the PCs. Selected from Ref. [75]. (f) 41 wavelengths; (g) 50 wavelengths. Selected from Ref. [76].

fiber to inhabit mode competition and hopping, and the MWFL operation is finally obtained.

Feng *et al.* demonstrated stable CW multi-wavelength operation in an EDFL with the aid of the NPR structure, as displayed in Figs. 6(c) and 6(d). By adjusting the position of PCs, there is a 28-wavelength laser output with a wavelength spacing of 0.8 nm[73]. From the output spectrum, the power distribution is uniform over a wide spectral range, which is well suited for DWDM sources. The experiment indicated that the setup of NPR is a favorable power equalizer.

The NALM cavity contains a Sagnac interferometer and a ring cavity combined with a coupler, which can also be named a figure-of-eight cavity. The working principle of multi-wavelength operation based on NALM is the same as NPR. The Sagnac interferometer also forms the comb filter effect[79], and the transmission equation of the Sagnac loop can be expressed as

$$T = 1 - 2\alpha(1-\alpha)\{1 + \cos[\phi + (1-2\alpha)\phi_{\mathrm{NL}}]\}, \quad (4)$$

where α is the coupling rate of couplers, $\phi_{\mathrm{NL}} = \gamma P_0 L$ is the nonlinear phase shift, γ is the nonlinear parameter, P_0 is the incident power in the Sagnac loop, and L is the loop length. The NALM structure also induces intensity-dependent loss as the NPR structure. Therefore, the NALM probably achieves multi-wavelength operation.

Feng *et al.* demonstrated a multi-wavelength CW EDFL with the aid of an NALM structure behaving as an amplitude equalizer[76]. The number of wavelength operation of lasers launched was up to 50, and the wavelength spacing was 0.8 nm. More interestingly, the spectrum amplitude jitter was slight [see Figs. 6(f) and 6(g)], which also suits the DWDM system.

NPR and NALM structures introduce intensity-dependent cavity loss and form the comb filter effect in a fiber laser cavity in order to obtain multi-wavelength operation. More interestingly, the two structures also can balance the amplitude of every wavelength, and a uniform amplitude MWFL is obtained, which is favorable for DWDM communication systems.

D. Multi-Wavelength CW Operation Based on the Nonlinear Effect

With a high-power laser transmitting in fiber, it is easy to produce a remarkable nonlinear effect such as self-phase modulation (SPM), cross-phase modulation (XPM), four-wave mixing (FWM), and stimulated Brillouin scattering (SBS). The FWM effect, a third-order nonlinear response process in medium, can prominently contribute to realizing multi-wavelength operation[80–82].

The FWM effect makes energy of each wavelength transfer among them, and power is again redistributed through a fast FWM process. The fast FWM effect is achieved when low-power wavelength laser intensity increases and high-power wavelength laser intensity reduces, which can effectively restrict longitudinal mode competition and hopping introduced by uniform broadening of the gain fiber. Accordingly, stable MWFLs can be produced through the FWM effect[18,33,82–87].

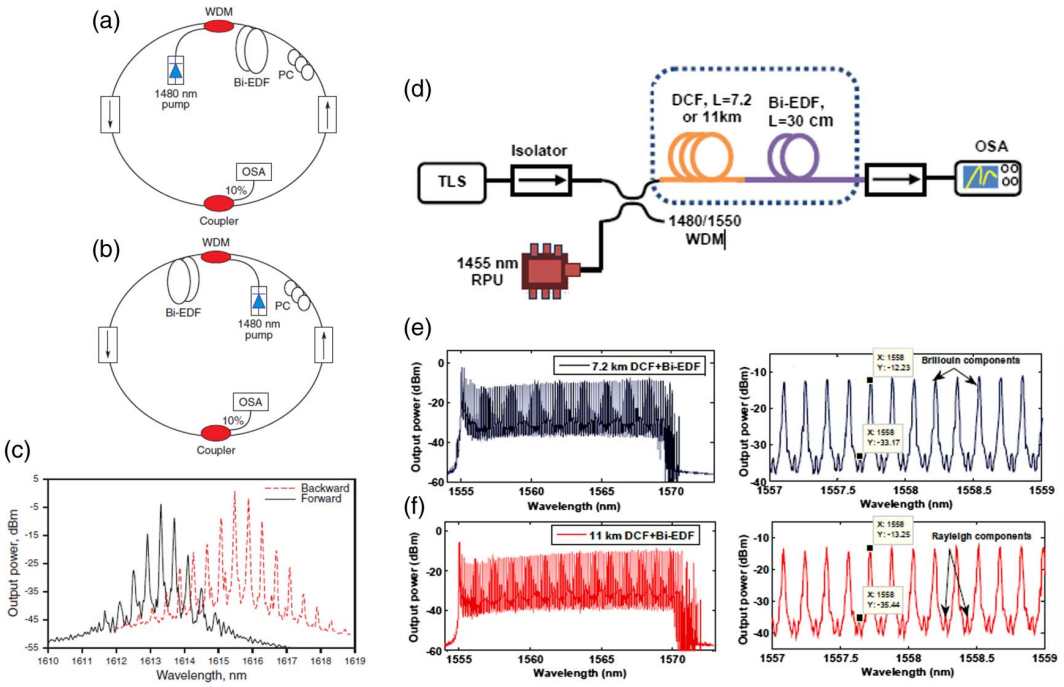

Fig. 7. Multi-wavelength operation in the ring EDFL: (a) the experimental setup of backward pumping; (b) the experimental setup of forward pumping; (c) the output spectrum of forward and backward pumping. Selected from Ref. [83]. The multi-wavelength Brillouin–Raman fiber laser: (d) the experimental setup; (e) and (f) illustrations of multi-wavelength lasing spectra at different DCF lengths. The magnified views are shown in graphs on the right. Selected from Ref. [34].

Liu *et al.* experimentally demonstrated and explained in detail that FWM can achieve multi-wavelength operation[33]. Harun *et al.* reported multi-wavelength EDFL by inserting a piece of bismuth-based Er-doped fiber (Bi-EDF) in the resonator[83]. A fiber laser, having up to 17 wavelengths with a fixed wavelength spacing of 0.41 nm, was realized, as shown in the Figs. 7(a)–7(c). The oscillating laser wavelengths interact with each other and continuously create new photons at other frequencies via the FWM process, which results in multi-wavelength operation. Yang *et al.* reported stable MWFLs based on a sampled fiber Bragg grating (SFBG) and the FWM effect, which was induced by a highly nonlinear photonic crystal fiber (HNL-PCF). Correspondingly, the dual-, triple-, and quintuple-wavelengths operation fiber laser was successfully obtained[84].

In addition, the SBS effect continuously generates new-order Stokes frequency when the power exceeds the Brillouin threshold and can stimulate Stokes lines[34,88–90]. Mamdoohi *et al.* demonstrated a kind of tunable multi-wavelength Brillouin–Raman fiber laser[34]. For pursuing more Stokes lines emission, they optimized Raman pump power and Brillouin pump power, so up to 195 Brillouin Stokes lines are generated, as shown in the Figs. 7(d)–7(f).

Stimulating the FWM or SBS effect generally needs a high-power laser and high nonlinearity medium. Therefore, the MWFL can be generated by adding a high nonlinearity fiber (HNLF)[18,82,86], photonic crystal fiber (PCF)[84], and dispersion compensation fiber (DCF)[85] to induce high nonlinearity effect.

In conclusion, the different methods have different advantages. For example, the number of multi-wavelengths achieved by the NPR or NALM structure is relatively large, and the amplitude of each wavelength is relatively uniform. The multi-wavelength operation achieved by FBGs that possess a designed reflection bandwidth can precisely control which wavelength emits, and the narrow filter linewidth is suitable to achieve SLM operation. The multi-wavelength operation based on the SMS structure or FWM effect can achieve a simple and compact experimental setup.

3. MULTI-WAVELENGTH PULSED FIBER LASER

Over the past decades, the pulsed fiber laser has been widely studied due to large pulse energy, ultrashort pulse duration, excellent beam quality, low cost, simple structure, and good compatibility[5,91–99]. At present, the pulsed fiber laser mainly divides two classifications by their principles: Q switching[98–102] and mode locking[94,103–105]. The Q-switching technique is a modulation process of the quality factor Q of the resonant cavity, while the mode-locking technique induces a fixed phase difference depending on the length of the resonant cavity between adjacent longitudinal modes.

On the other hand, there are also two main categories of pulsed fiber lasers based on different pulse generation technologies: active modulation techniques[106–111] and passive modulation techniques[112–118] of pulsed fiber lasers. Active modulation technology applies electronic devices controlled by an outside driving power source and adjusts the loss or phase in the cavity to achieve pulsed laser operation. Different from active modulation, passive modulation applies the nonlinear absorption characteristic of an SA that makes the CW transform into pulsed light. Compared with active modulation technology, the passive modulation fiber laser does not need additional electronic devices; thus, it causes more interest due to lower cost and the simple and all-fiber structure. The multi-wavelength pulsed fiber laser is probably achieved when multi-wavelength and pulsed laser generating technology work together.

In general, there are mainly three ways to achieve a multi-wavelength pulsed fiber laser, including active modulation techniques, adding wavelength or intensity-dependent loss structure to the cavity, and applying the high nonlinearity effect of two-dimensional (2D) materials. We mainly introduce multi-wavelength mode-locked fiber lasers (MWMLFLs) based on passive modulation technology.

A. Multi-Wavelength Pulsed Fiber Laser Based on NPR or NALM Structure

The pulsed MWFL, especially passively MWMLFL, has been comprehensively demonstrated due to its wide range of practical applications from civilian to military. Nowadays, passively mode-locked devices are roughly divided two types: real and artificial SAs. Artificial SA structures including NPR[78,119–124] and NALM[125–130], which apply the nonlinear refractive index and birefringent characters of fiber to induce nonlinear saturable absorption depending on light intensity, simulate the mode-locking process of real SAs. As expounded above, NPR and NALM structures introduce wavelength or intensity-dependent loss (i.e., tuning the cavity transmission) in the resonant cavity and restrain the intensive mode competition resulting from homogeneous gain broadening. Accordingly, multi-wavelength operation and the mode-locked pulse are probably simultaneously obtained in one fiber laser that is only based on the NPR or NALM setup.

Tang *et al.* established a theoretical model of NPR mode locking based on the complex nonlinear Schrodinger equation (NLSE) and revealed the evolution process of a pulse[120]. Stable MWMLFLs have been intensively reported, where output wavelengths range from 1 to 2 μm. Xu *et al.* numerically and experimentally demonstrated an all-normal-dispersion dissipative soliton (DS) mode-locked Yb-doped fiber laser (YDFL)[31] with the tri-wavelength operation. A stable tri-wavelength operation with fixed 16.4 nm spacing between adjacent peaks was obtained. Song *et al.* demonstrated steady dual-wavelength and tri-wavelength mode-locked operation in an EDFL[122]. The interval between the two adjacent peaks was switchable: 12.67 nm (1584.15–1571 nm), 33.32 nm (1595.52–1562.2 nm), and 43.4 nm (1559.04–1602.44 nm), by adjusting the orientation of the PCs.

Yan *et al.* demonstrated tri-wavelength operation in a TDFL with the aid of an NPR structure[78]. Three cases of switchable tri-wavelength mode-locked operation (see Fig. 8) were obtained by changing the value of θ_1, θ_2, and B_m via finely tuning the positions of the PCs. Luo *et al.* combined the NPR structure and a semiconductor SA mirror (SESAM) to achieve hybrid mode locking, which could more easily obtain stable multi-wavelength mode-locked operation[123]. It is worth mentioning that they added the 1.6 m polarization-maintaining fiber (PMF) with a fiber birefringence of 4.11×10^{-4} enlarging it two orders of magnitude over the SMF to decrease spacing of the adjacent transmission peak. Finally, up to seven wavelengths in the communication band were obtained.

In the NALM structure fiber laser, the Sagnac interferometer also forms a comb filter, which contributes to multi-wavelength operation. However, compared with the MZI and SMS interferometer, the NALM setup can alone achieve multi-wavelength operation without another mode-locking structure.

Plenty of MWMLFLs were also demonstrated based on the NALM structure. He *et al.* demonstrated a tunable

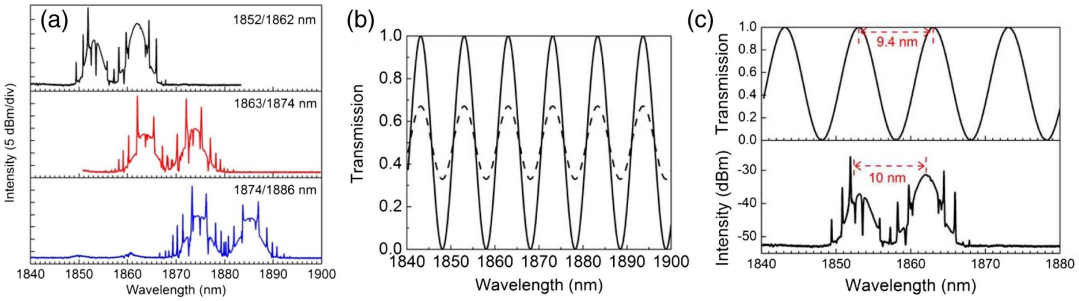

Fig. 8. Spectrum characteristic of the dual-wavelength TDFL: (a) the three-states switchable dual-wavelength conventional soliton; (b) the numerical simulation transmission spectrum of the NPR; (c) the comparison between simulative and experimental results. Selected from Ref. [78].

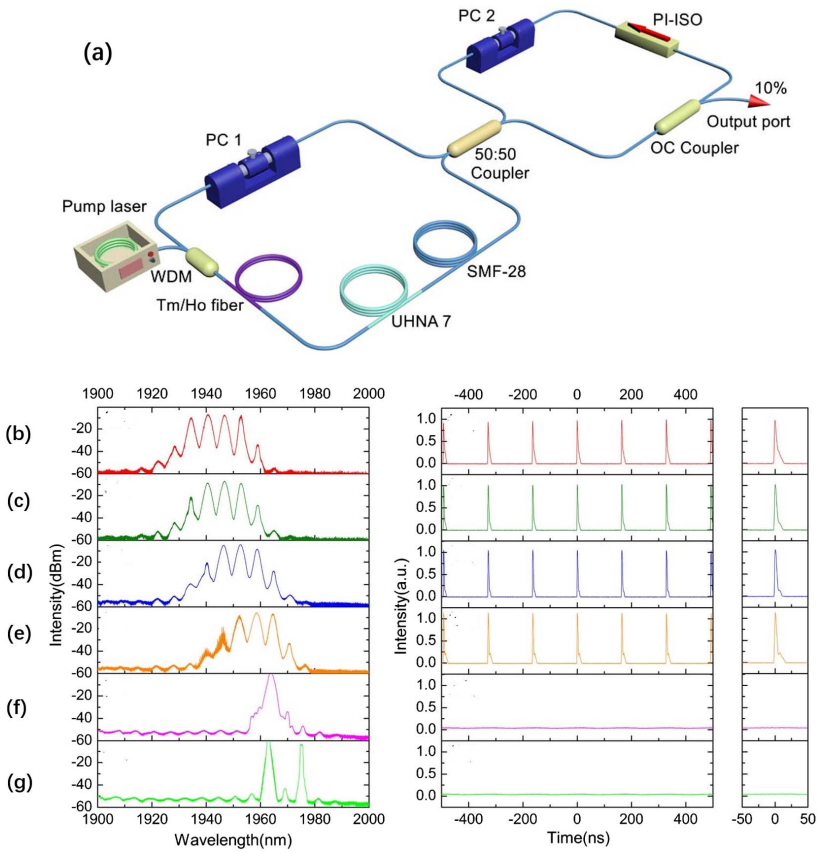

Fig. 9. Schematic and laser characteristics of the NALM fiber laser: (a) the schematic diagram of a mode-locked Tm/Ho-doped fiber laser; (b)–(e) tunable multi-wavelength spectrum (left), corresponding pulse trace (middle), and single pulse (right); (f) and (g) show CW operation characteristics. Selected from Ref. [126].

multi-wavelength TDFL-based Sagnac loop filter[131]. They placed a PMF in the Sagnac loop to shorten the interval of adjacent peaks. Furthermore, they deduced the spacing between adjacent channels as

$$\Delta\lambda = \frac{\lambda^2}{\Delta n L}, \tag{5}$$

where Δn is a birefringence index, and L is the length of PMF in the Sagnac loop.

Jin *et al.* applied the NALM structure in the TDFL to achieve stable tunable four-wavelength mode-locking operation[126], where the separation between adjacent channels maintains 6 nm whether there is mode locking or CW operation, as shown in Fig. 9.

In addition, researchers combined filter devices and active modulation technology to achieve multi-wavelength mode-locking operation. Jain *et al.* demonstrated a five-wavelength mode-locked-operation-based active Mach–Zehnder intensity modulator under 10 GHz driving signal frequency[29]. The stable ultrashort pulse was obtained, where the pulse width is 14 ps, and the repetition rate is 10 GHz. The MWFL with an ultrahigh repetition rate is suited to high-speed and large-capacity optical fiber communication systems.

B. Multi-Wavelength Pulsed Fiber Laser Based on 2D Materials

A real SA[43,45,132,133], possessing excellent nonlinear absorption characteristics depending on light intensity, has been intensively studied to realize a Q-switched or mode-locked fiber laser. In 2004, graphene was first discovered by the simple method of mechanical exfoliation. For a dozen years, 2D materials have been intensively studied in many fields such as photonics, chemistry, mechanics of materials, and other interdisciplinary fields because of their peculiar and excellent properties[96,134–139]. In 2D materials, the covalent bond intensively holds the atoms within every layer of material, while the weak van der Waals force exists in adjacent layers. Accordingly, the single- and few-layer structures 2D materials can be easily obtained from bulk material by physical stress (e.g., centrifugation, stir, exfoliation, and ultrasonic). The 2D materials family members are successively discovered in recent years, such as topological insulators (TIs)[44,140–144], hexagonal boron nitride (h-BN)[145–148], transition metal dichalcogenides (TMDs)[149–153], black phosphorus (BP)[154–162], phosphorene[95,163], antimonene[164–166], MXenes[167–171], metal–organic frameworks (MOFs)[172–174], and covalent organic frameworks (COFs)[175,176], as shown in Fig. 10(a).

Nowadays, 2D materials have been extensively applied in the field of photonic devices, especially as mode lockers to generated ultrashort pulses in fiber lasers due to their broadband absorption, fast carrier dynamics, ease of fabrication, ease of integration into the cavity, and highly nonlinear optical saturable property. The SA is the key device for mode-locked fiber lasers, and the current dominant SAs, as shown in Fig. 10(b), have nonlinear saturable absorption characteristics, depending on the intensity [see Fig. 10(c)].

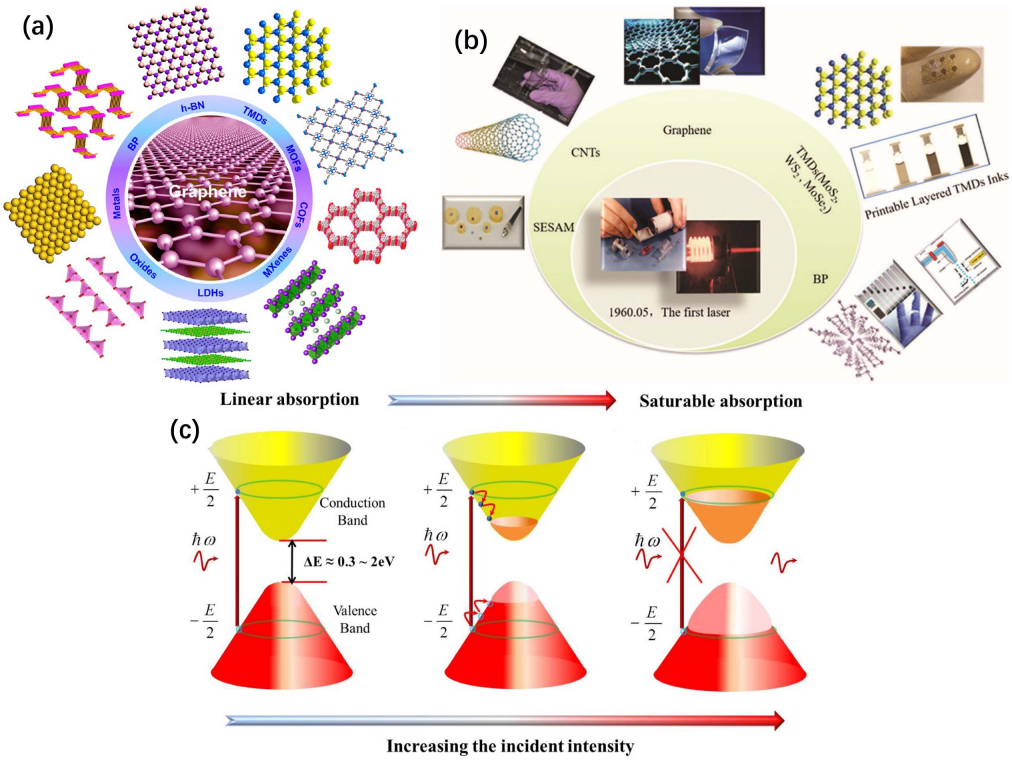

Fig. 10. 2D materials. (a) The 2D family members. Selected from Ref. [135]. (b) The current dominant SAs for ultrashort-pulse generation. Selected from Ref. [136]. (c) The sketch map of the saturable absorption process in the BP. Selected from Ref. [154].

Martinez *et al.* summarized the methods of integrating graphene or carbon nanotubes (CNTs) with fiber, as shown in Fig. 11[177]. However, these methods are universal for other 2D materials. For example, researchers homogeneously mingle 2D material nanosheets and film-forming agents [e.g., polyvinyl alcohol (PVA), polymethyl methacrylate (PMMA)] to comprise a sandwich structure, which can be perfectly added between two fiber connectors [see Fig. 11(a)]. Besides, researchers coat 2D materials on the surface of D-shaped fibers, as shown in Fig. 11(d), or tapered fibers, as shown in Fig. 11(e), which utilize the evanescent field to interact between light and materials. The sandwich structure, D-shaped, or tapered fibers are ideal carriers for 2D materials, and these structures realize the all-fiber laser format, which prevents tedious alignment work.

There are a few methods of transferring 2D materials on the surface of a fiber such as optical deposition[178–180] or pulse laser deposition (PLD)[44,181]. Finally, 2D materials are deposited on the waist of the tapered fiber, the fiber ends, or the surface of the D-shaped fiber, and added into the cavity as an SA. The D-shaped fiber and tapered fiber belong to the microfiber, and light interacts with materials through the evanescent field.

In past decades, SESAMs have been comprehensively used in fiber lasers for mode-locked[182–184] or *Q*-switched[185,186] pulse operation. SESAMs have excellent and stable performances benefited by advanced semiconductor technologies such as excellent bandgap and defect engineering and precise growth technologies. These technologies allow accurate control with the SA parameters (such as recovery time, modulation depth, unsaturated loss, and saturation fluence). However, the SESAM has inherent disadvantages, such as narrow-band operation (only absorbing the designed wavelength band), complexity, high cost, and complex fabrication. Therefore, a new-style SA with excellent and versatile characteristics is urgently desired[131].

On the other hand, 2D materials process high third-order nonlinear susceptibility, which generates a remarkable nonlinear effect. As expounded upon above, the FWM effect obviously mitigates mode competition and stabilizes the multi-wavelength operation. Hence, 2D materials have double functions: as a mode locker resulting from natural saturable absorption properties and a multi-wavelength generator resulting from a high nonlinear refractive index ($\sim 10^7$ larger than SiO_2)[187], respectively. Therefore, a multi-wavelength mode-locking fiber laser possibly can be exploited by only adding a 2D materials SA in the cavity.

Graphene, a type of one-atom-thick layered graphite, processes a zero bandgap structure, full waveband absorption, and short recovery time characteristics, so it can work as a SA to achieve mode-locked operation[6,178,179,188–197]. Hendry *et al.* have demonstrated that graphene can offer an ultrahigh third-order optical nonlinearity and generate a strong FWM effect with weak dependence on wavelength[198]. Hence, optical power will redistribute in different wavelengths, which efficiently mitigates the mode competition and stabilizes the multi-wavelength operation. The strong FWM effect of graphene with an ultrathin thickness could have the ability to stablize multi-wavelength lasing of fiber lasers. Moreover, graphene can be fabricated with a flexible, low-cost production process compared to SESAM and can be well compatible with fibers.

Luo *et al.* experimentally confirmed that graphene can generate FWM and obtained stable five-wavelength *Q*-switching operation in the YDFL and 23-wavelength *Q*-switching operation in the EDFL[199]. They considered that graphene acts in a dual role, as a mode locker and multi-wavelength stabilizer based on the FWM effect. Zhao *et al.* experimentally realized the dual-wavelength rectangular pulses in YDFL by only applying a microfiber-based graphene SA, as shown in Fig. 12[196]. Furthermore, the switchable dual-wavelength fiber laser was also successfully obtained by finely rotating the PCs.

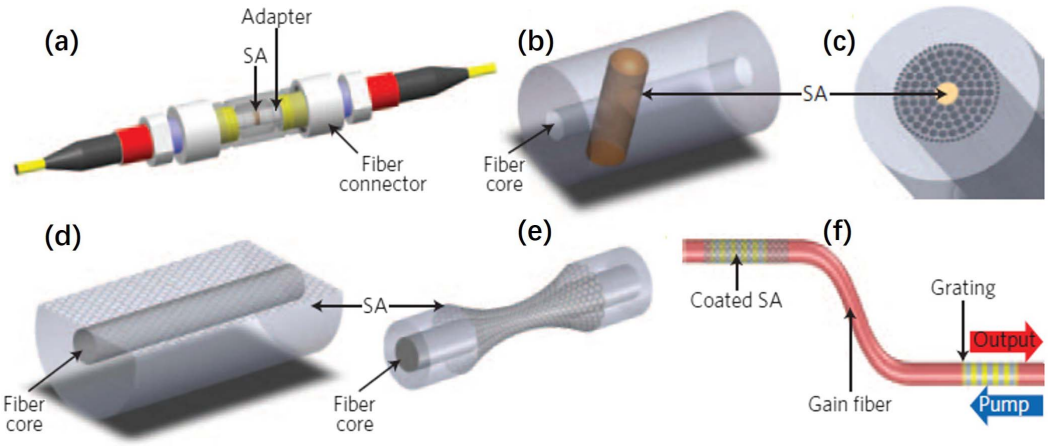

Fig. 11. Diverse methods of integration of CNT-/graphene-SAs into the resonant cavity: (a) sandwiched film between two fiber connectors; (b) in-fiber microfluidic channels; (c) PCFs filled by the SA; (d) D-shaped fiber; (e) tapered fiber; (f) fully integrated monolithic fiber laser. Selected from Ref. [177].

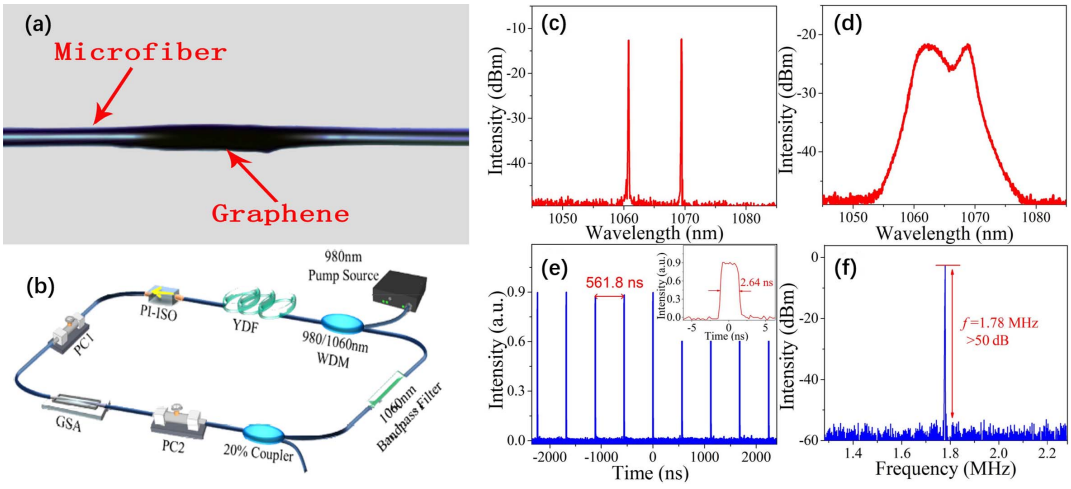

Fig. 12. Characteristics of dual-wavelength YDFL-based graphene SA (GSA): (a) microscopy image of tapered fiber-based GSA; (b) the schematic diagram of dual-wavelength YDFL; (c) the spectrum of dual-wavelength CW operation; (d) the spectrum of mode-locked operation; (e) the oscilloscope trace, inset: single-pulse envelope; (f) the RF spectrum. Selected from Ref. [196].

Zhao *et al.* prepared the available graphene-oxide-PVA film as a mode locker, which was inserted into the EDFL cavity. They successfully obtained dual-wavelength at 1572.93 nm and 1588.37 nm, respectively.

These carbon-based materials, as the SA applied in an ultrafast fiber laser, are easily damaged under high-power laser exposing, which limits practical applications. Hence, looking for other materials to replace graphene to achieve mode-locked working is a hot issue. TIs, a typical direct bandgap 2D material, have a narrow bandgap (0.2–0.3 eV) with a wide absorption bandwidth[200–210]. TIs also have outstanding saturable optical absorption features and a high three-order nonlinear refractive index that work together to generate a multi-wavelength mode-locked pulse. Zhang *et al.* applied the Z-scan to research and analyze optical nonlinear properties of Bi_2Te_3 and Bi_2Se_3[210,211], and found that the TI possesses high three-order nonlinearity characteristics. These characteristics have the potential to be applied in the photonic field at both the optical and microwave bands, which is proved by plenty of research achievements.

Guo *et al.* applied home-made few-layer TI:Bi_2Se_3 to make a TI-SA by optical deposition[212]. A tri-wavelength mode-locked EDFL based on a TI-SA was generated, as shown in Fig. 13.

TMDs, a novel 2D family member, also possess ultrafast optical nonlinear properties[131,152,153,213–221]. TMDs have a diverse combination (compound), and they may behave

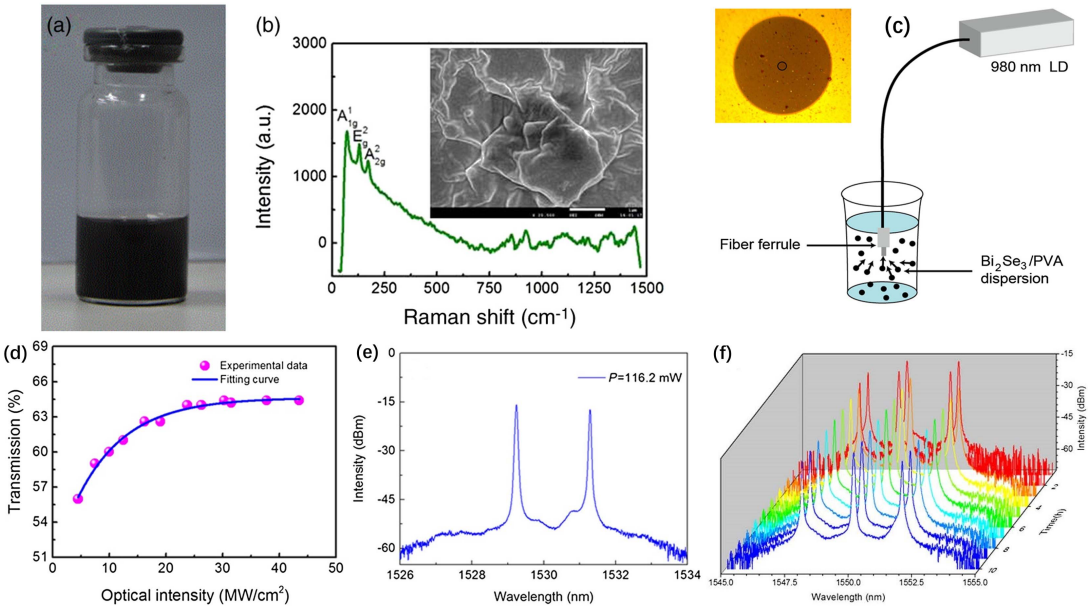

Fig. 13. TI-SA and characteristics of MWMLFL: (a) the solution of Bi_2Se_3/PVA; (b) Raman spectrum of Bi_2Se_3/PVA, inset: scanning electron microscope (SEM) image; (c) optical deposition process, inset: photo of the end of the fiber; (d) the saturable absorption characteristic of TI-SA; (e) the output spectrum under 116.2 mW pump power; (f) long-time output wavelength stability measurement of the tri-wavelength mode-locking operation over 9 h. Selected from Ref. [212].

as three different states: metallic, semiconducting, or insulating. TMDs have a tunable bandgap according to different layers of TMDs. MoS_2, one of the typical materials of TMDs, has an indirect 1.29 eV bandgap (bulk state). However, single-layer MoS_2 becomes a direct bandgap, and the bandgap increases to 1.90 eV[222]. Fortunately, TMDs have a wide absorption range, even exceeding the fundamental absorption bandwidth due to sub-bandgap saturable absorption. Wang *et al.* utilized the open-aperture Z-scan technique to investigate the ultrafast nonlinear optical property of MoS_2[223]. In the experiment process, under the same excitation condition, they demonstrated that MoS_2 possesses better saturable absorption response performance than graphene dispersions. Hence, TMDs have the same strongly nonlinear absorption characteristics as graphene and can be used as an SA to apply in an ultrafast laser.

Guo *et al.* applied a high-power pulsed laser beam to deposit WS_2 on the surface of a fiber taper[224]. This device was added into the EDFL, and the single- and dual-wavelength operations were successfully demonstrated by finely adjusting the pump power and PCs. Finally, the dual-wavelength mode-locked fiber laser working at 1558.54 nm and 1565.99 nm was successfully obtained (see Fig. 14).

Recently, BP, a thermo-dynamically stable allotrope of phosphorus, walks into researchers' field of vision due to excellent properties[136,155,162,225–232]. The property of 2D-layer BP is very similar to graphene, which is all constituted by a single element. BP is a kind of direct bandgap semiconductor with high charge carrier mobility and tunable bandgap value characteristics. The value of bandgap energy depends on the number of layers distributing from 2.0 eV (single layer) to 0.3 eV (bulk materials).

Lu *et al.* applied the wide-band Z-scan measurement technique to demonstrate that BP has broadband and enhanced saturable absorption characteristics, as shown in Fig. 15[154]. They thought that multi-layer BP could be

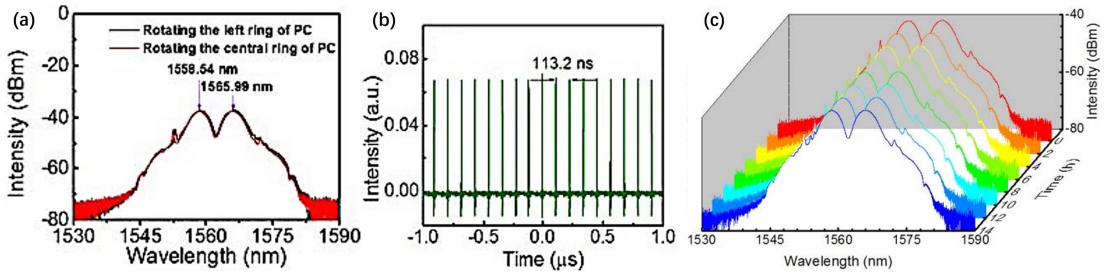

Fig. 14. Output properties of dual-wavelength EDFL: (a) the spectrum of the dual-wavelength EDFL; (b) the pulse traces; (c) long-term output spectrum stability measurement. Selected from Ref. [224].

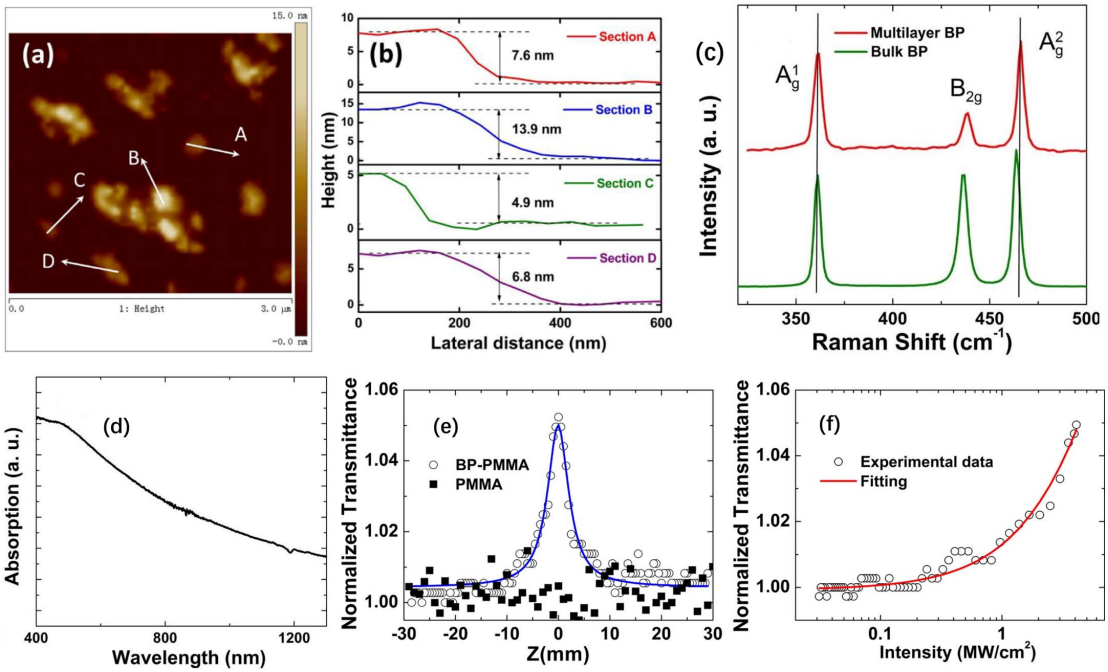

Fig. 15. Characteristics of BP nanoparticles (NPs): (a) the atomic force microscope (AFM) image; (b) height profiles of the sections marked in (a); (c) Raman spectrum; (d) the linear absorption spectrum; (e) the Z-scan measurements of BP-PMMA film; (f) the relation of normalized transmittance and intensity. Selected from Ref. [154].

exploited as a new type of high-performance SA with wide absorption bandwidth, which was verified by plenty of research work.

The same as other 2D materials discussed above, BP also possesses strong saturable absorption and high nonlinear refractive index characteristics. Zhao *et al.* demonstrated stable tri-wavelength mode-locking operation in the EDFL-based few-layer BP-SA[233]. They removed the BP-SA and observed the output spectrum characteristics [see Figs. 16(c) and 16(d)]. The output spectrum alters unstably, and the number of wavelengths also changes without the BP-SA in the cavity. However, the output tri-wavelength spectrum could remain stable for 25 min with the aid of a BP-SA in the cavity. BP-SA acts as a power stabilizer and really contributes to multi-wavelength operation by contrast experiments. Yun experimentally generated a dual-wavelength mode-locked vector conventional soliton based on BP-SA[234], and the central wavelengths are at 1533 and 1558 nm, respectively, with a pulse width of about 700 fs.

In addition, some researchers combined the real SA and filter devices to realize MWMLFL. Liu *et al.* demonstrated a tri-wavelength mode-locked fiber laser with the aid of a single-walled CNT (SWCNT) SA and three CFBGs working together[48]. The output three wavelengths operate at about 1540, 1550, and 1560 nm, corresponding to three central wavelengths of CFBGs (see Fig. 17). The corresponding pulse widths are 6.3 ps, 6.7 ps, and 5.9 ps, respectively.

In the 2D materials multi-wavelength mode-locked fiber laser (see Table 1), the SA is required to have the saturable absorption effect and high nonlinear refractive index. Only providing a remarkable nonlinear effect by SA, the strong FWM effect makes optical power redistribute at different wavelengths and efficiently mitigates the mode competition. The 2D materials have enormous advantages in the multi-wavelength mode-locked fiber laser due to the simple and compact structure and lower cost.

C. Other Optical Phenomena with Multi-Wavelength Pulsed Operation

There are a few different optical phenomena accompanying multi-wavelength pulsed operation, such as wavelength tuning[29,122,212], wavelength switching[69,121,123], bright–dark soliton pair[235], and different kinds of soliton pulses[31,132,182]. For example, the tunable or switchable multi-wavelength operation can be obtained in three different operation modes, CW, Q-switched, and mode locked modes, by properly adjusting PCs and pump power in a proper position, as shown in the experimental remarks of Tables 2 and 3. For example, the transmittance of the NPR structure, sensitive to polariton states in the cavity, reaches the maximum value when $\Delta\varphi_N + \Delta\varphi_{\mathrm{NL}} \approx \Delta\varphi_N = 2\pi N$ and is expressed by

$$N = LB_m/\lambda. \tag{6}$$

The spacing between adjacent peaks of transmission $\Delta\lambda$ is shown as

$$LB_m\left(\frac{1}{\lambda} - \frac{1}{\lambda + \Delta\lambda}\right) = 1. \tag{7}$$

In theory, the spacing between adjacent peaks and the position of the transmission peak change with birefringence of fiber and polarization states. Therefore, tunable

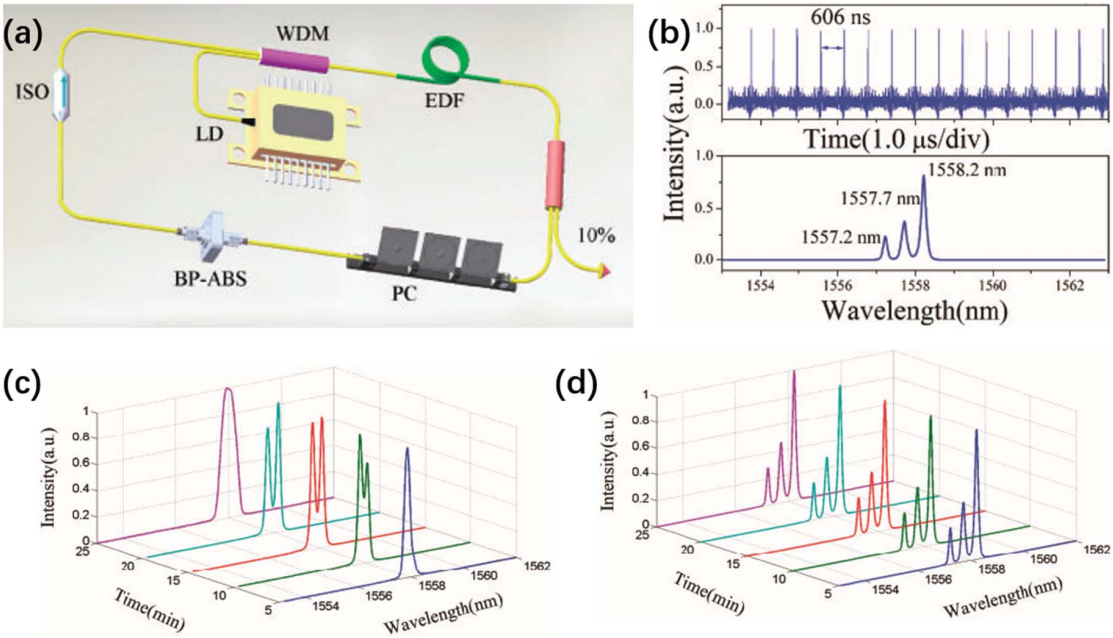

Fig. 16. Output characteristics of tri-wavelength mode-locking based on the BP-SA: (a) the schematic of the EDFL; (b) the characteristics of the pulse trace (up) and spectrum (down); the emission spectrum of the EDF (c) without and (d) with BP-SA. Selected from Ref. [233].

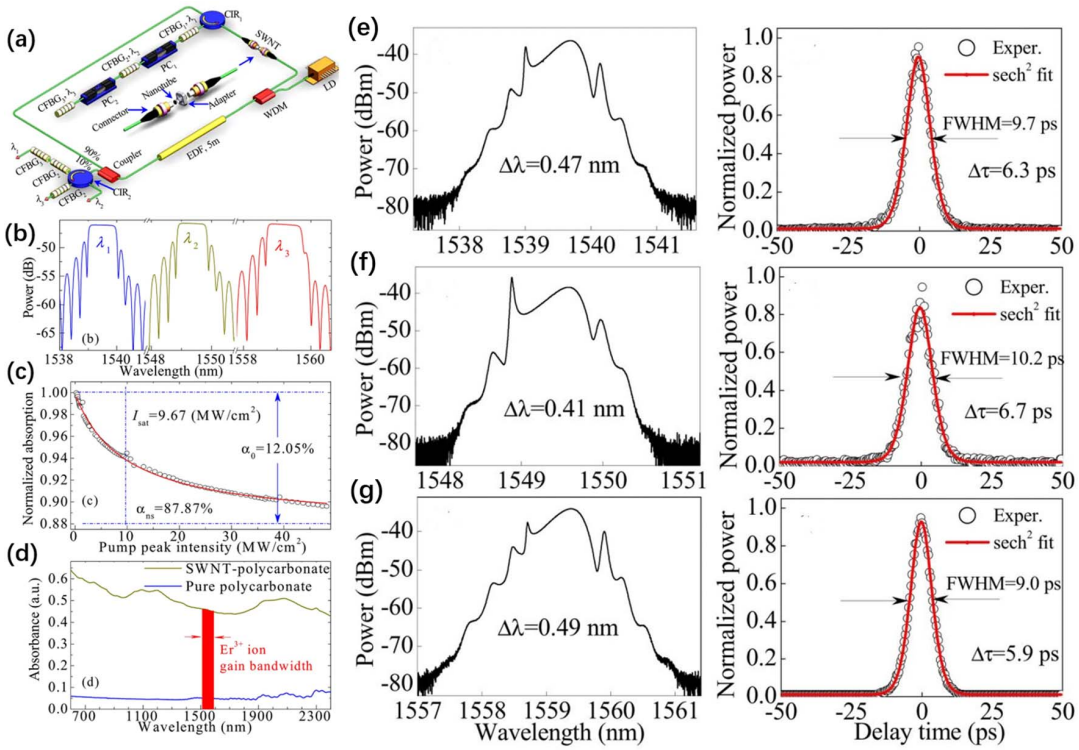

Fig. 17. Schematic diagram and laser output characteristics of the fiber laser: (a) the schematic of the tri-wavelength mode-locked fiber laser; (b) the measured reflection spectra of three CFBGs; (c) the normalized absorption characteristic of the SWCNT-SA; (d) linear absorption characteristic of the SWCNT-SA; (e)–(g) the output spectrum and corresponding autocorrelation intensity trace of λ_1, λ_2, and λ_3, respectively. Selected from Ref. [48].

Table 1. Summary of the Multi-Wavelength Pulsed Lasers Based on a Real SA

Type of 2D Materials	Work Mode	Integration Methods	Wavelength Range (nm)	Number of Wavelengths	Repetition Rate (MHz)	Pulse Duration (ps)	Ref.
Graphene	ML	PLD on taper	1529–1535.4	4	8.034	8.8	[188]
Graphene	ML	Optical deposition	1061.8, 1068.8	2	1.78	1410	[108]
Graphene	ML	Optical deposition on fiber taper	1031.43, 1034.94, 1038.43	3	0.55	74.6	[189]
Graphene oxide	ML	GO-PVA film	1056.5, 1062.3, 1069.5	3	14.2	340	[80]
Graphene oxide	ML	GO-PVA film	1572.93, 1588.37	2	23.54	12,200	[132]
TI: Bi_2Se_3	ML	Bi_2Se_3-PVA film	1567.2, 1568, 1568.7, 1569.5	4	8.83	22	[67]
TI: Bi_2Te_3	ML	Optical deposition on fiber end	1548, 1550, 1552	3	8.95	~30	[212]
TMDs: WS_2	ML	Optical deposition on fiber taper	1568.55, 1569	2	2.14	11	[222]
TMDs: WS_2	ML	PLD on taper	1558.54, 1565.99	2	8.83	0.6	[224]
BP	ML	BP film	1572.2, 1557.7, 1558.2	3	1.65	16.99	[233]
BP	ML	BP-PVA film	1533, 1558	2	20.8	0.7	[234]
CNT+FBG	ML	CNT-PVA film	1540, 1550, 1560	3	6.18	6.3, 6.7, 5.9	[48]

Table 2. Summary of the MWFL Based on the Filter Effect in the Cavity

Working Principle	Wavelength Range (nm)	Number of Wavelengths	Spacing (nm)	3 dB Linewidth (nm)	Power Fluctuation (dB)	Ref.	Remark
MZI	1558.6–1559.2	2	0.6	0.02	<0.43	[26]	Wavelength tunable
MZI	1545–1556	29	0.4/0.8	–	<1	[27]	Spacing tunable
MZI	1534–1534.4	3	0.2	<0.05	<0.912	[53]	Wavelength switchable
SMS	1560.8–1563.9	2	3.1	<0.136	<0.46	[30]	Wavelength tunable
SMS	1894.17–1904.21	3	~5	<0.04	<2	[57]	–
FBG	1569.38–1569.6	2	~0.2	–	–	[59]	Wavelength tunable and switchable
FBG	1559.80, 1560.65, 1561.25	3	–	0.07	–	[61]	–
NPR	1550–1575	28	0.8	0.04	<0.2	[73]	Spacing tunable
NALM	~1967–1981	42	0.33	–	<1	[75]	–
FWM	1562–1605	50	0.8	<0.05	–	[76]	–
FWM	~1555–1561.5	9	0.8	0.05	<1.2	[84]	Spacing tunable
FWM	1555.68–1561.41	7	0.95	–	0.18	[18]	–
SBS	~1561–1572	11	1	–	1	[86]	Spacing tunable
Interaction of SRS, SBS, RS	~1555–1570	195	0.16	–	–	[34]	Wavelength tunable

Table 3. Summary of the Multi-Wavelength Mode-Locked Lasers Based on NPR or NALM

Structure	Wavelength Range (nm)	Number of Wavelengths	Repetition Rate (MHz)	Pulse Width (ps)	Ref.	Remark
NPR	~1040–1074	3	36	–	[31]	Wavelength tunable
NPR	1852/1862, 1863/1874, and 1874/1886	2	2.68	–	[78]	Wavelength switchable
NPR+ PS-LPFBG	1031.48–1056.32	3	2.5	460	[119]	Wavelength tunable
NPR	1902.5–1917.3	3	14.7	1.36	[121]	–
NPR	1571.48/1584.15	2	10.23	9.4/8.6	[122]	Spacing tunable
NPR	~1560–1585	7	7.44	5.68	[123]	Wavelength tunable and switchable
NPR	1865–1887	3	2.68	–	[124]	Wavelength switchable
NALM	1570–1604	20	1.434	5490	[125]	–
NALM	1935–1953	4	6.1	3700	[126]	Wavelength tunable
MZI modulation	1545.52–1561.28	5	10000	14	[29]	Wavelength switchable

or switchable MWMLFL can probably be generated based on the NPR structure.

Yan *et al.* reported a switchable tri-wavelength mode-locked TDFL with the aid of the NPR technique, as shown in Fig. 18[124]. The stable tunable one-by-one single-wavelength output and switchable pair-by-pair dual-wavelength output were successfully achieved by properly adjusting the position of the PCs.

The tunable or switchable fiber lasers as stated have huge potential applications in optical signal processing, fiber sensors, and WDM communication systems. When it comes to tunable or switchable fiber lasers, no matter

whether it is CW or mode-locked operation, the polarization state is inevitably mentioned. When parameters of cavity (e.g., θ_1, θ_2, and B_m) change, the transmittance characteristics (the position of the peak or spacing of the adjacent peak) will be altered. Therefore, tunable or switchable MWFLs are finally obtained. As for switchable or tunable MWFLs based on nonlinear optical loop mirrors (NOLMs) or filter devices, they are also very sensitive to polarization states in the cavity. Hence, it is crucial to adjust the polarization state to a proper position in the tunable or switchable fiber lasers.

In the mode-locked fiber laser, there are generally four kinds of solitons: conventional soliton[236–240], dispersion managed soliton[128,240–243], similariton[244–248], and dissipative soliton[144,189,237,249–251] based on the different dispersion environments in the cavity. MWMLFLs also can operate with different solitons. For example, tri-wavelength dissipative solitons based on a graphene SA in a YDFL and dual-wavelength conventional soliton mode-locking based on WS_2-SAs were reported by researchers, which indicates that the 2D material is a kind of versatile and powerful material.

Huang *et al.* reported stable multi-wavelength dissipative soliton YDFLs based on a graphene-oxide SA[132]. The fiber laser achieved abundant experimental phenomena of tunable dual-wavelengths, spacing-tunable dual-wavelength, and wavelength switchable DSs, as shown in Figs. 18(d)–18(h). From the Fig. 18(h), we can clearly see that the polarization states indeed affect the wavelength-switching process.

What is discussed above is all bright pulses, but there is another pulse type: the dark pulse, which can also be generated in the fiber laser. The dark pulse, a localized intensity dipping on the CW background, has significant potential application in optical communication due to lower loss. Zhang *et al.* experimentally achieved stable dark soliton operation from an all-normal-dispersion fiber laser[252]. They also numerically analyzed dark solitons based on the NLSE. Since then, dark solitons are part of numerous experiments successively springing up based on the NPR structure[253] and real SA[72,235,254,255]. Ning *et al.* demonstrated the bright–dark pulse pair based on the NALM setup[256]. They experimentally found that the pulse pair is formed because of the intensive cross-coupling

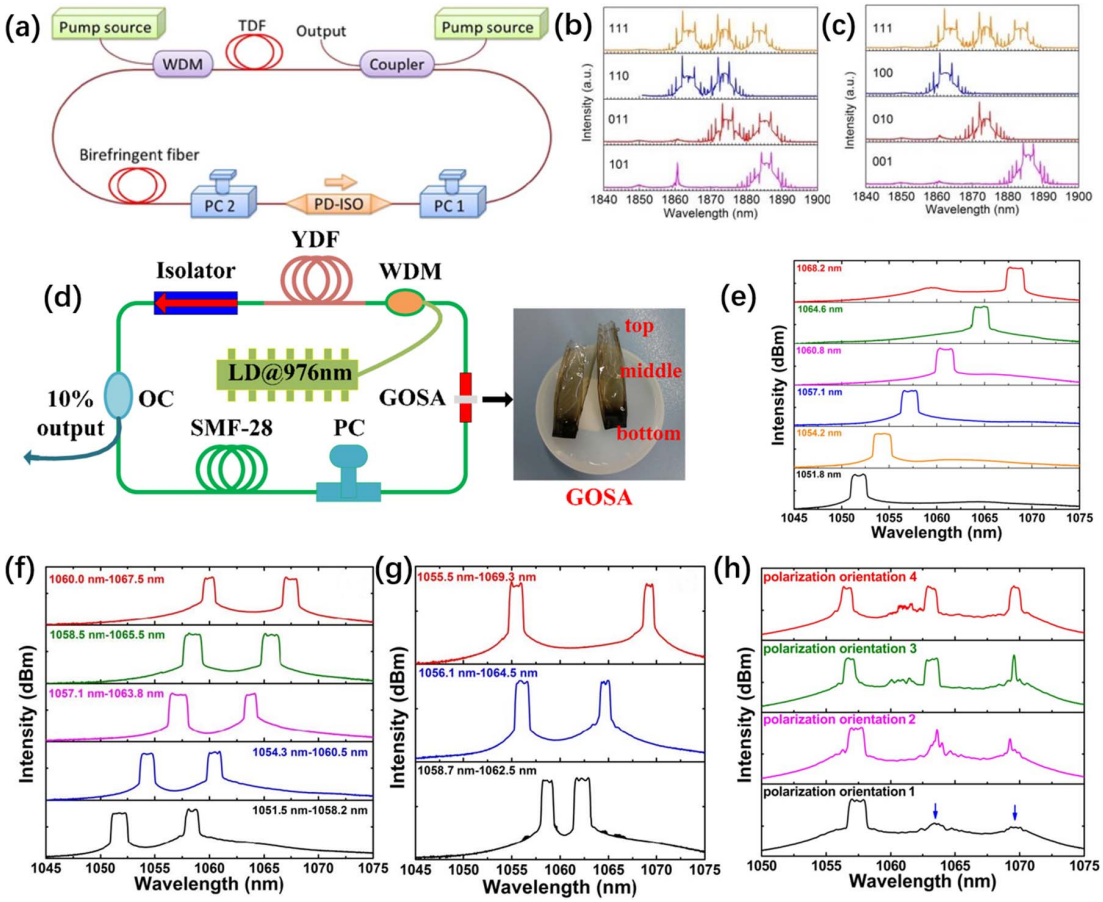

Fig. 18. Switchable multi-wavelength mode-locked TDFL: (a) the experimental setup; the spectrum of the switchable tri-wavelength of (b) pair-by-pair and (c) one-by-one. Selected from Ref. [124]. (d) The schematic of the YDFL based on a graphene-oxide (GO)-SA, and spectral characteristics of tunable multi-wavelength DS; (e) the tunable single-wavelength spectra; (f) the wavelength-tunable dual-wavelength DSs; (g) the spectrum of spacing-tunable dual-wavelength DSs; (h) the switchable spectrum dynamics of tri-wavelength DSs by adjusting the orientation of the PC. Selected from Ref. [132].

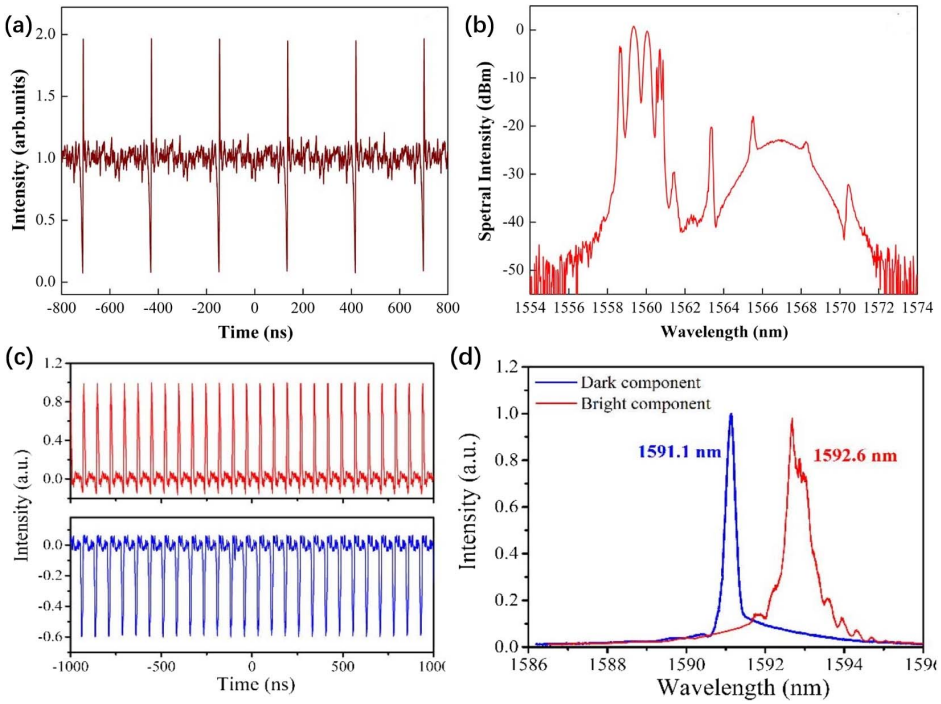

Fig. 19. Laser characteristics of a bright–dark soliton pair based on NALM structures: (a) oscilloscope pulse traces and (b) the corresponding optical spectrum. Selected from Ref. [257]. The laser characteristics of the bright–dark pulse based on the ReS_2–SA: (c) the pulse trace of a bright pulse (up) and dark pulse (down) and (d) corresponding optical spectrum, respectively. Selected from Ref. [72].

effect between the bright and dark pulses and is located at two different wavebands (see Fig. 19).

Except for the bright–dark pair achieved by NALM, the bright and dark pair fiber laser also may be obtained with real SA. Zhao *et al.* experimentally demonstrated a dual-wavelength bright and dark pulse pair based on ReS_2 (a member of TMDs) SA[72]. They studied the characteristics of bright and dark pulses, respectively, through an outside cavity PC and a tunable filter dividing each other. They found that the bright and dark pulses possess different wavelengths and polarization states.

In conclusion, abundant experimental phenomena have been obtained in fiber lasers, which indicates that fiber lasers are powerful, versatile, and ideal platforms for studying peculiar nonlinear evolution processes. The tunable and switchable MWFL operating in CW or pulsed forms can achieve different wavelength emission based on different requirements, which greatly extend the application ranges.

4. DUAL-CAVITY DUAL-WAVELENGTH PULSED FIBER LASER

The MWFL discussed above is based on single-gain medium in the resonant cavity, and the multi-wavelength operation principle suppresses mode competition and hopping of the gain fiber. There is other way to achieve two-color pulse operation, which is the dual-cavity structure fiber laser. Every cavity has an independent gain medium and pump source. The wavelength intervals between different gain media are large. There is no gain competition between the two wavelengths, so dual-wavelength operation may be obtained in the dual-cavity fiber laser. Compared with the MWFL based on a single-gain fiber, the dual-cavity structure fiber laser can achieve two-color operation in a wider range. Moreover, the two wavelengths have their own independent tuning range in the gain bandwidth.

Dual-wavelength fiber lasers, especially two-wavelength pulsed operation at the same repetitive frequency, have extensive applications such as nonlinear frequency conversion, pump–probe technique, chemical sensing, and Raman scattering spectra, owing to their compact structure, stable operation, excellent heat dissipation, and excellent beam quality[197,257,258]. In recent years, the passively synchronous dual-wavelength pulsed fiber laser has attracted much attention. There are mainly three methods to synchronize two beams with different wavelengths based on the cross-absorption modulation effect of materials, the XPM effect of fiber, and the gain-switched effect.

A. Passively Synchronized Mode-Locked Dual-Wavelength Fiber Laser Based on Cross-Absorption Modulation of Materials

As we know, graphene has excellent nonlinear saturable absorption characteristics, which acts as a mode locker applied in the fiber laser. When two-beam lasers with different wavelengths simultaneously illuminate graphene, the transmittance of one beam light is not only affected by its own light intensity, but is also affected by the light intensity of another beam, which is called the cross-absorption modulation effect, as shown in Fig. 20.

Dual-wavelength passively synchronized Q-switched or mode-locked fiber lasers can be achieved based on the

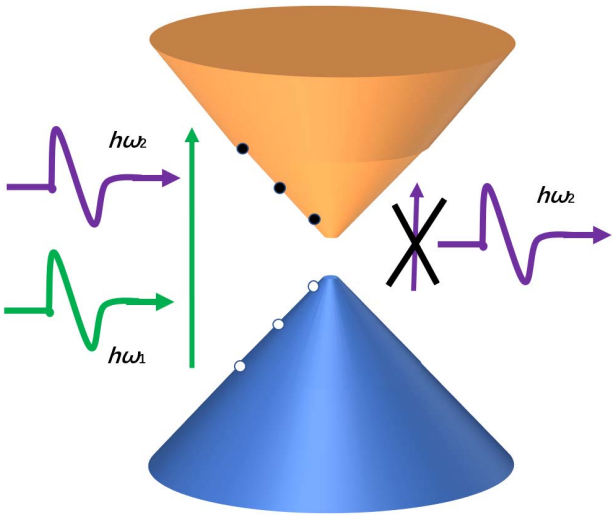

Fig. 20. Schematic of cross-absorption modulation in graphene.

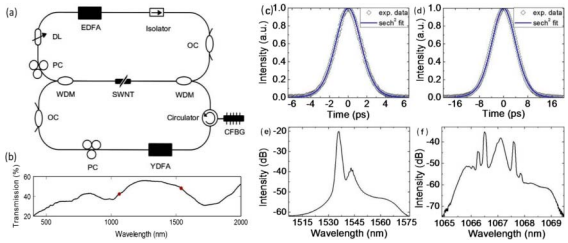

Fig. 21. Passively synchronized two-color fiber laser with the aid of SWCNTs: (a) the experimental setup of the fiber laser; (b) linear transmission of SWCNTs; (c) the intensity autocorrelations of the Er laser; (d) the intensity autocorrelations of the Yb laser; (e) the corresponding spectrum of the Er laser; (f) the corresponding spectrum of the Yb laser. Selected from Ref. [257].

cross-absorption modulation effect of materials. Jia *et al.* reported a two-color synchronized *Q*-switched TM^{3+}-doped ZrF_4-BaF_2-LaF_3-AlF_3-NaF (ZBLAN) fiber laser emission at 1.48 μm and 1.85 μm, respectively, based on a common graphene SA[259]. They also successfully achieved two-color simultaneous mode-locking operation at a different repetition rate. Zhang *et al.* used the cross-absorption modulation effect of SWCNTs to achieve 1/1.5 μm synchronized mode-locked pulse output with an identical repetition frequency of 13.08 MHz, as shown in Fig. 21[257].

In the dual-cavity passively synchronized fiber laser, the SA devices shall have a wide wavelength saturable absorption bandwidth covering gain fiber emission wavelength and be placed on the public area of the dual cavity.

B. Passively-Synchronized Dual-Wavelength Fiber Laser Based on the XPM Effect

When two or more beams of light with different frequencies transmit in the fiber at the same time, they will interact through the nonlinear effect in the fiber, which is called XPM. From the perspective of physics, the effective refractive index of light waves in a medium is not only related to its own intensity, but also related to the intensity of other waves transmitted at the same time, which is the reason for the generation of XPM. Due to the XPM effect in fiber, a nonlinear phase shift related to the intensity can be obtained, as shown in the formula

$$N_j^{\mathrm{NL}}(z) = n_2\left(\frac{\omega_j}{c}\right)(|E_j|^2 + 2|E_{3-j}|^2)z. \tag{8}$$

On the right-hand side of the equation, the first item stems from the self-phase modulation effect, and the second item originates from XPM due to different frequency lights transmitting in the fiber.

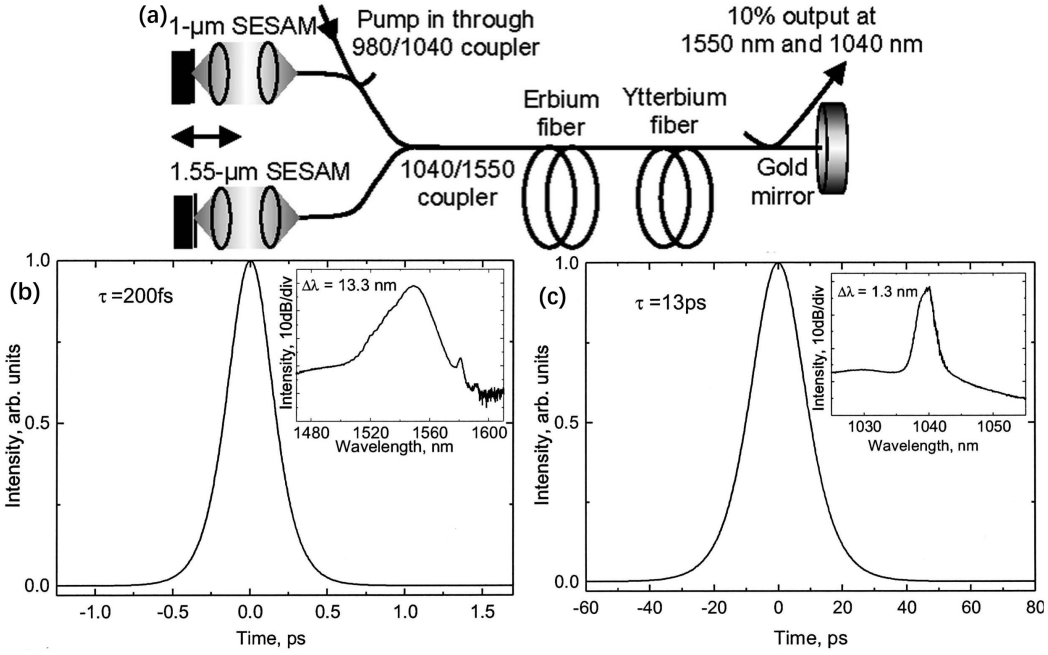

Fig. 22. Passively synchronized two-color fiber laser based on the XPM effect: (a) the schematic diagram of the fiber laser; (b), (c) intensity autocorrelation trace (inset: corresponding spectrum) of the Er laser and Yb laser. Selected from Ref. [258].

Rusu *et al.* proposed dual-wavelength synchronized mode-locked fiber lasers based on the XPM effect in a common linear cavity[258]. When the master pulse (1.55 μm) and slave pulse (1 μm) overlap temporally in the public area of the linear cavity, the spectrum of the slave pulse shifted because of intensive phase modulation afforded by the master pulse. The slave pulse's group velocity alters correspondingly, so the oscilloscope train of the slave pulse actively matches the master pulse. A two-color synchronized mode-locked fiber laser was obtained by the XPM effect, as shown in Fig. 22. In this experiment, the EDFL generated a master pulse due to its higher peak power and shorter pulse duration (200 fs), and the pulse of the YDFL acted as a slave pulse due to relatively longer pulse duration (13 ps).

In the dual-cavity two-color fiber laser, the XPM effect and cross-absorption modulation effect, all originating from third-order nonlinearity, may work together for passively synchronized mode-locking operation. Sotor *et al.* reported a two-color mode-locked fiber laser, including two ring cavities (Er- and Tm-doped) based on a common graphene SA placed in the public area of the dual cavity, as shown in Fig. 23[197]. Graphene has wide-band absorption and completely covers the gain bandwidth of the Er-doped fiber (EDF) and Tm-doped fiber (TDF). The graphene SA also acts in dual roles in the fiber laser as a mode locker and optical modulator. The 1558.5 nm and 1938 nm two-color mode-locked operation with the same repetition rate of 20.5 MHz was realized. The experiment results indicated that the graphene will

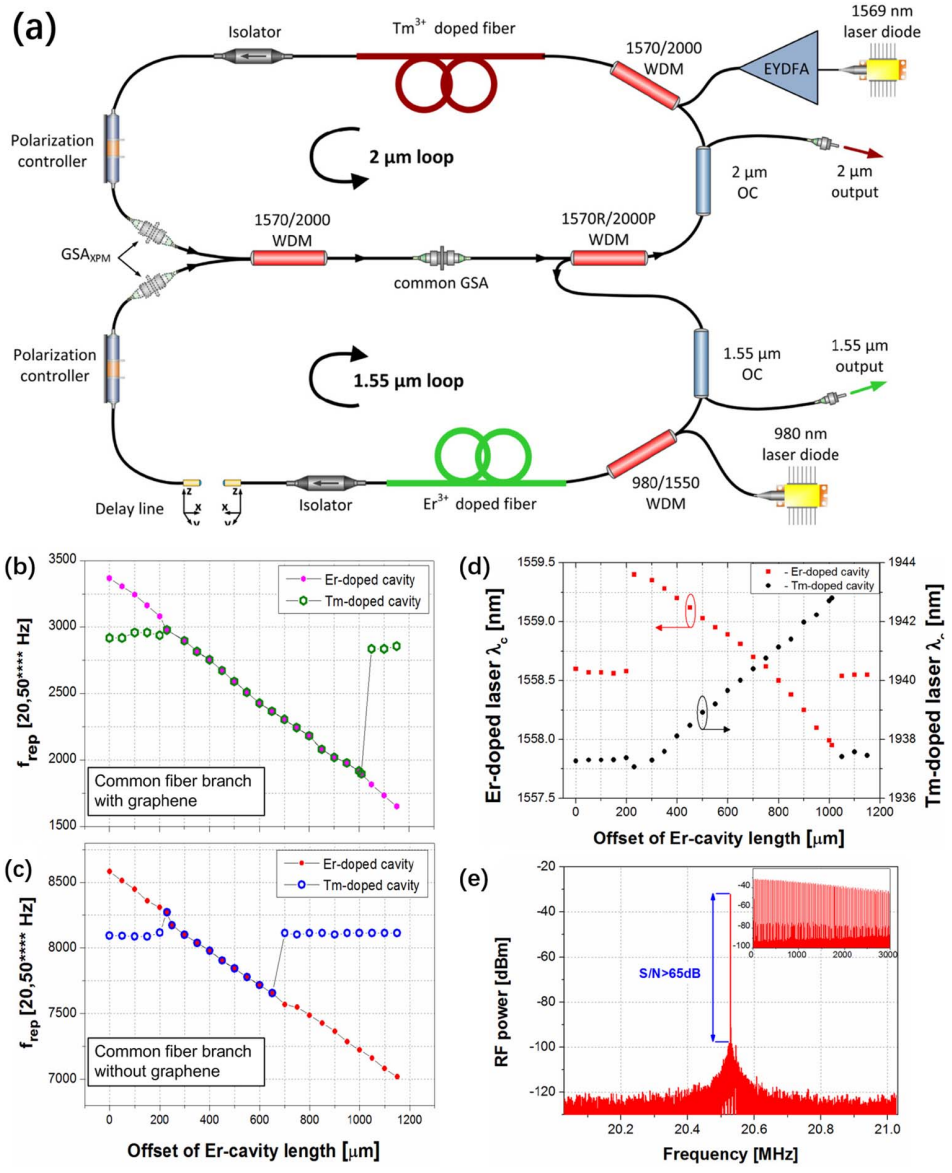

Fig. 23. Dual-wavelength dual-loop cavity passively synchronized mode-locked fiber laser: (a) the schematic diagram of the experimental setup; the relation between repetition rates of Er- and Tm-doped cavities and Er-cavity length offset (b) with a common GSA in the public area and (c) with two independent GSA_{XPM} in the different loops; (d) the central wavelengths versus the offset of Er-cavity length based on a common GSA; (e) the RF spectrum. Selected from Ref. [197].

Table 4. Summary of the Dual-Cavity Two-Color Mode-Locked Lasers

Type	Operation Mode	Central Wavelength (nm)	Repetition Rate (MHz)	Pulse Duration	Ref.
Cross-absorption modulation	Synchronized ML	1067.1/1535.48	13.08	6.1/2.1 ps	[257]
Cross-absorption modulation	Synchronized *Q*-switched	1480/1850	0.02	4.9 μs	[259]
XPM	Synchronized ML	1040/1540	29	13/0.2 ps	[258]
XPM + cross-absorption modulation	Synchronized ML	1558.5/1938	20.5	0.915/1.57 ps	[197]
Gained *Q*-switched	Synchronized *Q*-switched	1046/1546	0.0117	5.3/4.6 μs	[260]
Gained *Q*-switched	Synchronized *Q*-switched	2073.05/2954.7	0.108	0.85/0.99 μs	[261]

enhance the synchronization range through contrast experiments.

C. Dual-Wavelength Pulsed Fiber Laser Based on Gain-Switched Technology

What is discussed above are two gain fibers, where the two-color fiber laser can also be realized in a single-gain fiber processing two rare earth ions such as an Er/Yb co-doped fiber (EYDF) (see Table 4). There is an energy transfer process between two kinds of rare earth ions, achieving dual-wavelength working based on gain-switched technology. Guo *et al.* experimentally demonstrated 1046 nm and 1546 nm two-color dual-cavity fiber lasers based on a single EYDF, as shown in Fig. 24[260]. In the experiment, the 1 μm waveband *Q*-switched pulses are realized based on the saturable absorption effect of unpumped EYDF. In the EYDF, there is an energy transferring process from the $^2F_{5/2}$ level of Yb^{3+} to the $^4I_{11/2}$ level of Er^{3+} ions through non-radiative energy transfer. Therefore, the 1.5 μm pulses are finally achieved based on the gain switching of Er^{3+} ions introduced by the 1 μm *Q*-switched pulses.

EYDF exists in the non-radiative energy transferring process between the energy levels of Yb^{3+} and Er^{3+} ions. In the gain fiber, the cascade transitions process of rare earth ions also affords the potential to produce dual- or multi-wavelength emission. Li *et al.* reported a passively

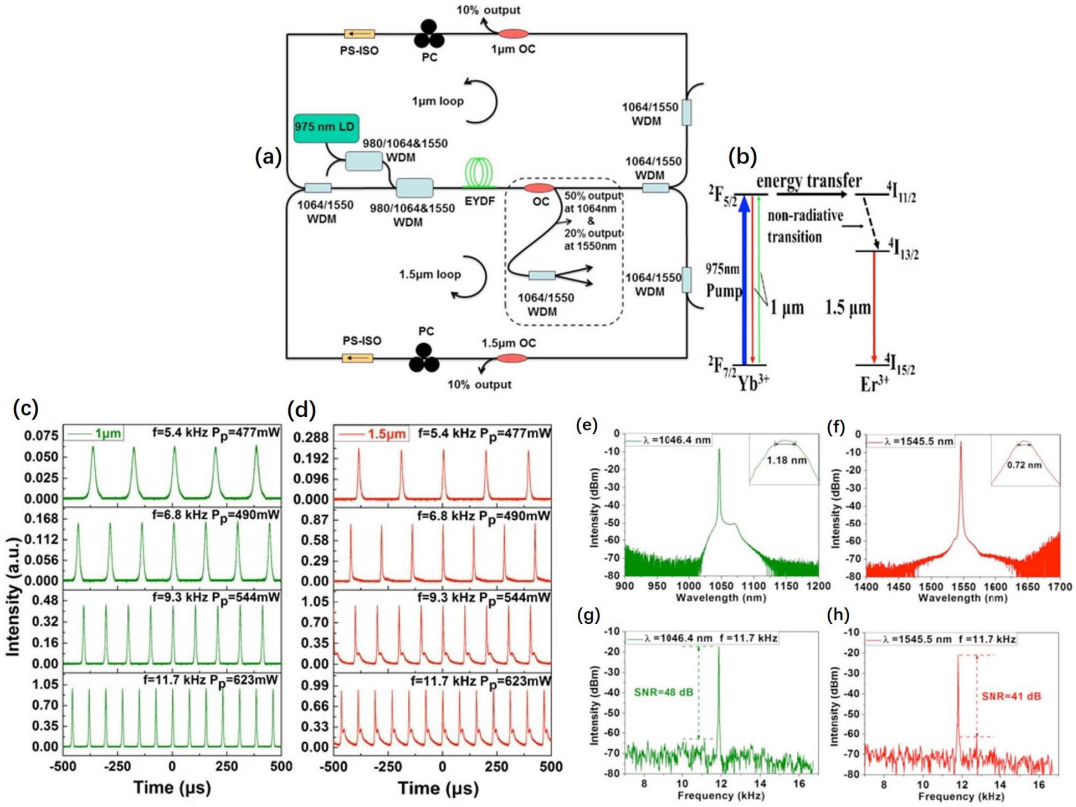

Fig. 24. Synchronized dual-cavity two-color *Q*-switched EYDF laser: (a) the schematic of the experimental setup; (b) the energy level diagram of the EYDF; *Q*-switched traces under different pumps of (c) 1 μm and (d) 1.5 μm; optical spectra of (e) 1 μm and (f) 1.5 μm; the corresponding RF spectra of (g) 1 μm and (h) 1.5 μm. Selected from Ref. [260].

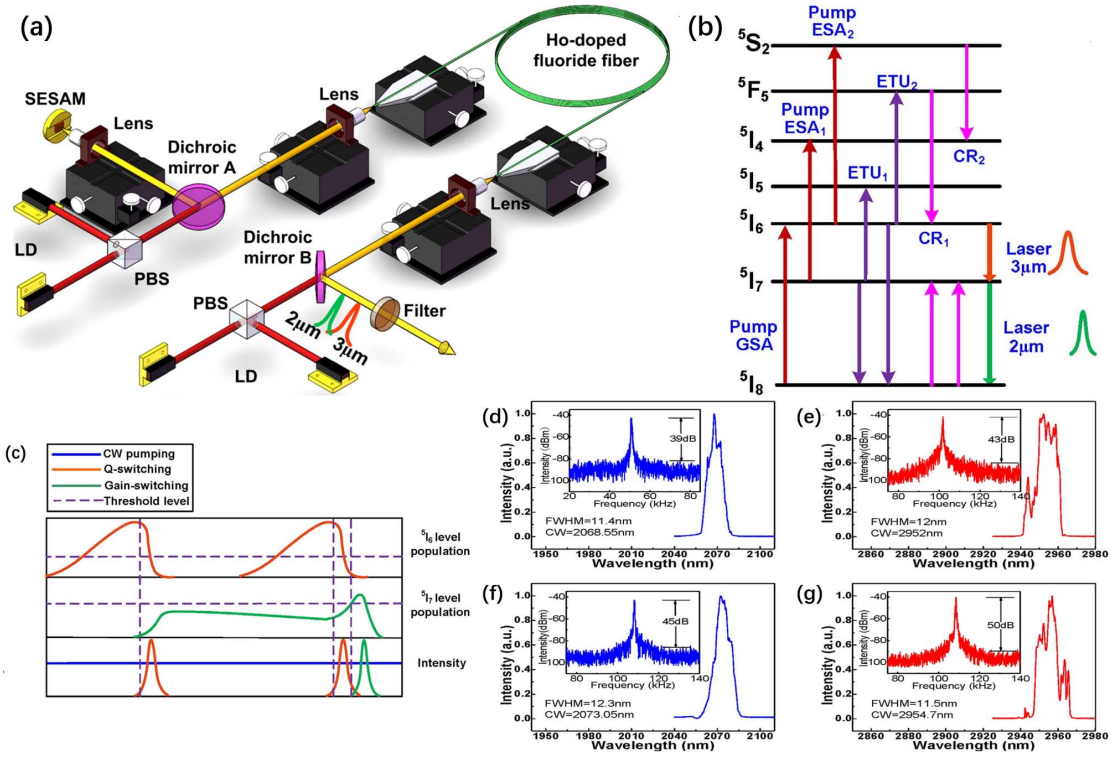

Fig. 25. Dual-wavelength Ho^{3+}-doped fluoride fiber laser: (a) the experimental setup; (b) the energy level of the cascade transition process; (c) the illustration of laser upper-level populations of $^6I_5$ and $^5I_7$, respectively, and the temporal domain evolution of pulse intensity; the characteristics of optical and corresponding RF spectra (inserted) at the different pump powers of (d), (e) at 3.76 W and (f), (g) at 6.47 W, respectively. Selected from Ref. [261].

Q-switched pulse operating at ~3 μm and a gain-switched pulse operating at ~2 μm in a common cavity with a Ho^{3+}-doped fluoride fiber as gain media (see Fig. 25)[261].

In the passive dual-cavity synchronized mode-locked fiber laser, it is very necessary to ensure exactly equivalent lengths to meet the same repetition rate. If not, two-color Q-switched or mode-locked fiber lasers will operate at different repetition rates.

5. CONCLUSION AND PERSPECTIVE

Among the kinds of fiber lasers, the multi-wavelength mode-locked fiber laser has been intensively investigated due to plentiful practical applications from civilian to military. There are a few methods to realize MWMLFLs. Researchers insert a fiber interferometer to form the comb filter effect. However, they cannot obtain multi-wavelength mode-locking operation due to the lack of other mode-locked devices. NPR and NALM structures figure out the question due to simultaneously processing mode-locker and comb filter dual effect. NPR or NALM structures induce wavelength or intensity-dependent loss, which is helpful for multi-wavelength operation. However, the spectral bandwidth of the mode-locked multi-wavelength laser is relatively small, and the pulse duration is relatively large. Stable multi-wavelength mode-locking operation can be achieved based on the 2D materials SA. 2D materials possess peculiar characteristics of broadband saturable absorption and high nonlinearity effect, which are indispensable for multi-wavelength mode-locking operation. Until now, the MWMLFL have been demonstrated with the aid of the multiple 2D materials SA, for example, graphene, TI, TMDs, and BP.

In the future, we predict that the MWMLFL will develop in five directions as follows.

1) More reliable and stable 2D materials: Researchers can exploit more 2D materials family members and realize a multi-wavelength mode-locked-operation-based 2D materials SA. Recently, a novel 2D material MXene[167,169,262–264] entered researchers' eyes. We firmly hold that MXene also can be applied in mode-locked fiber lasers as a mode locker. MXene possesses many advantages such as hydrophilicity, metallic conductivity, and adjustable chemical composition compared with other typical 2D materials. Achieving stable, reliable, uniform, and large-scale produced 2D materials[265–268] is a very challenging issue in the whole world. However, it is very important to get stable multi-wavelength mode-locked fiber lasers with the aid of a reliable 2D materials SA.
2) More stable laser output performance: A comb filter and reliable SA can work together to achieve a stable multi-wavelength ultrafast laser, which give play to both advantages (ultranarrow band-pass linewidth of filters and a reliable, stable mode-locked SA)[48,123,269]. Stable multi-wavelength mode-locked fiber lasers can meet practical applications. Accordingly, successfully

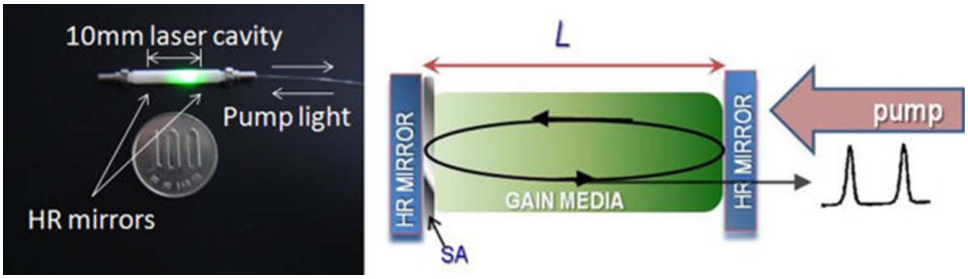

Fig. 26. Ultrashort-cavity fiber laser. Selected from Ref. [280].

transferring the laboratory achievements to marketable applications will bring immeasurable economic benefits.

3) Longer operation wavelength: At present, MWFLs typically focus on the spectral region around 1 μm and 1.5 μm, which limits their applications. We can utilize other gain media to achieve longer wavelength operation. Mid-infrared light sources cover numerous strong molecular absorption features[270–275], so mid-infrared fiber lasers have many applications, such as material processing, biomedical science, sensors, defense, and nonlinear mid-infrared photonics. For fiber lasers, Er- or Ho-doped fluoride fibers are ideal gain media for 3 μm[186,231,276–279], and the MWFL can sufficiently achieve mid-infrared operation in virtue of the methods summarized above.
4) More compact: The mode-locked fiber laser cavity can be packaged in 10 mm via ultrahigh rare-earth-doped concentrations and extra small graphene SAs, and the repetition frequency can reach 10 GHz, as shown in Fig. 26[280]. The micro-cavity mode-locked fiber laser combines FG technology to achieve a more compact-scale fiber source. On the other hand, benefitting from mature silicon-based optoelectronics technology, the integrated laser chip[281,282] that covers silicon-based optical waveguides, silicon-based modulators, and silicon-based light sources probably achieves a compact-scale multi-wavelength laser source.
5) More intelligent: In the fiber laser, the interval of adjacent output wavelengths and the number of wavelengths are sensitive to the polarization states in the resonant cavity. However, pure manual polarization state control is very tough to land on multi-wavelength mode-locked regimes, and the state of multi-wavelength mode locking is easily broken due to mechanical vibration and the external environment. Recently, automatic mode locking based on fast polarization searching has been achieved through genetic and evolutionary optimization algorithms[283,284]. Moreover, the automatic mode-locked fiber laser applying machine learning and deep learning has also been intensively demonstrated[285,286]. If the technology is applied in the multi-wavelength mode-locked fiber laser, the number of wavelengths and the peak position of the output wavelength can be intelligently controlled (see Fig. 27).

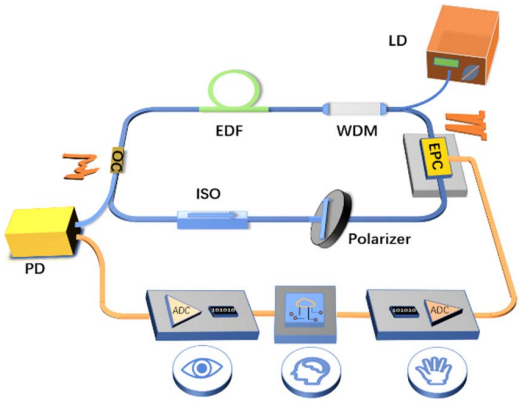

Fig. 27. Schematic diagram of the intelligent MWMLFL.

The research was partially supported by the Science and Technology Development Fund, Macao Special Administration Region (SAR) (Nos. 007/2017/A1 and 132/2017/A3), National Natural Science Foundation of China (NSFC) (Nos. 61875138, 61435010, 61775142, and 6181101252), Science and Technology Innovation Commission of Shenzhen (Nos. KQTD2015032416270385, JCYJ2015062 5103619275, and JCYJ20170811093453105), and Shenzhen Basic Research Project on Subject Layout (No. JCYJ2017 0412105812811). The authors also acknowledge the support from the Instrumental Analysis Center of Shenzhen University (Xili Campus).

†These authors contributed equally to the paper.

References

1. U. Keller, Nature **424**, 831 (2003).
2. X. Jiang, W. Li, T. Hai, R. Yue, Z. Chen, C. Lao, Y. Ge, G. Xie, Q. Wen, and H. Zhang, NPJ 2D Mater. Appli. **3**, 34 (2019).
3. H. Zhang, S. B. Lu, J. Zheng, J. Du, S. C. Wen, D. Y. Tang, and K. P. Loh, Opt. Express **22**, 7249 (2014).
4. Y. Song, X. Shi, C. Wu, D. Tang, and H. Zhang, Appl. Phys. Rev. **6**, 021313 (2019).
5. J. Liu, Y. Chen, P. Tang, C. Xu, C. Zhao, H. Zhang, and S. Wen, Opt. Express **23**, 6418 (2015).
6. D. Popa, Z. Sun, F. Torrisi, T. Hasan, F. Wang, and A. C. Ferrari, Appl. Phys. Lett. **97**, 203106 (2010).
7. H. Hillmer and B. Klepser, IEEE J. Quantum Electron. **40**, 1377 (2004).
8. C. A. Brackett, IEEE J. Sel. Areas Commun. **8**, 948 (1990).
9. G. Sarlet, G. Morthier, and R. Baets, J. Lightwave Technol. **18**, 1128 (2000).

10. J. Yao, J. Yao, Y. Wang, S. C. Tjin, Y. Zhou, Y. L. Lam, J. Liu, and C. Lu, Opt. Commun. **191**, 341 (2001).
11. C. L. Zhao, X. Yang, C. Lu, J. H. Ng, X. Guo, P. Roy Chaudhuri, and X. Dong, Opt. Commun. **230**, 313 (2004).
12. Y.-G. Han, T. Tran, S.-H. Kim, and S. B. Lee, Opt. Lett. **30**, 1282 (2005).
13. J. Marshall, G. Stewart, and G. Whitenett, Meas. Sci. Technol. **17**, 1023 (2006).
14. H.-B. Jeon and H. Lee, J. Opt. Soc. Korea. **18**, 406 (2014).
15. M.-G. Suh, Q.-F. Yang, K. Y. Yang, X. Yi, and K. J. Vahala, Science **354**, 600 (2016).
16. J. Fu, D. Chen, B. Sun, and S. Gao, Laser Phys. **20**, 1907 (2010).
17. S. Pan, C. Lou, and Y. Gao, Opt. Express **14**, 1113 (2006).
18. P. Wang, D. Weng, K. Li, Y. Liu, X. Yu, and X. Zhou, Opt. Express **21**, 12570 (2013).
19. D. S. Moon, U.-C. Paek, Y. Chung, X. Dong, and P. Shum, Opt. Express **13**, 5614 (2005).
20. N. Park and P. F. Wysocki, IEEE Photon. Technol. Lett. **8**, 1459 (1996).
21. S. Yamashita and K. Hotate, Electron. Lett. **32**, 1298 (1996).
22. A. Bellemare, M. Karásek, M. Rochette, S. Lrochelle, and M. Têtu, J. Lightwave Technol. **18**, 825 (2000).
23. S. K. Kim, M. J. Chu, and J. H. Lee, Opt. Commun. **190**, 291 (2001).
24. K. Zhou, D. Zhou, F. Dong, and N. Q. Ngo, Opt. Lett. **28**, 893 (2003).
25. J. Vasseur, M. Hanna, J. M. Dudley, and J. R. Barry, IEEE Photon. Technol. Lett. **17**, 2295 (2005).
26. W. He, L. Zhu, M. Dong, X. Lou, and F. Luo, Laser Phys. **28**, 045104 (2018).
27. A.-P. Luo, Z.-C. Luo, and W.-C. Xu, Opt. Lett. **34**, 2135 (2009).
28. J. Vasseur, M. Hanna, J. Dudley, J.-P. Goedgebuer, J. Yu, G.-K. Chang, and J. R. Barry, IEEE J. Quantum Electron. **43**, 85 (2007).
29. A. Jain, N. Chandra, A. Anchal, and P. Kumar, Opt. Laser Technol. **83**, 189 (2016).
30. A. Khattak, G. Tatel, and L. Wei, Appl. Sci. **8**, 1135 (2018).
31. Z. W. Xu and Z. X. Zhang, Laser Phys. Lett. **10**, 085105 (2013).
32. L. Ma, Z. Kang, Y. Qi, and S. Jian, Laser Phys. **24**, 045102 (2014).
33. X. Liu, X. Zhou, and C. Lu, Opt. Lett. **30**, 2257 (2005).
34. G. Mamdoohi, A. R. Sarmani, A. F. Abas, M. H. Yaacob, M. Mokhtar, and M. A. Mahdi, Opt. Express **21**, 18724 (2013).
35. L. Jian, Y. Jianping, Y. Jian, and Y. Tet Hin, IEEE Photon. Technol. Lett. **16**, 1020 (2004).
36. Y. E. Jeong, J. Sahu, D. Payne, and J. Nilsson, Opt. Express **12**, 6088 (2004).
37. Q. Fang, J. Li, W. Shi, Y. Qin, Y. Xu, X. Meng, R. A. Norwood, and N. Peyghambarian, IEEE Photon. J. **9**, 1506107 (2017).
38. S. V. Firstov, S. V. Alyshev, K. E. Riumkin, M. A. Melkumov, O. I. Medvedkov, and E. M. Dianov, Opt. Lett. **40**, 4360 (2015).
39. V. Fortin, M. Bernier, S. T. Bah, and R. Vallee, Opt. Lett. **40**, 2882 (2015).
40. Y. Xu, Q. Fang, Y. Qin, X. Meng, and W. Shi, Appl. Opt. **54**, 9419 (2015).
41. H. Zhang, Q. Bao, D. Tang, L. Zhao, and K. P. Loh, Appl. Phys. Lett. **95**, 141103 (2009).
42. H. Zhang, D. Tang, R. J. Knize, L. Zhao, Q. Bao, and K. P. Loh, Appl. Phys. Lett. **96**, 111112 (2010).
43. Z. Tian, K. Wu, L. Kong, N. Yang, Y. Wang, R. Chen, W. Hu, J. Xu, and Y. Tang, Laser Phys. Lett. **12**, 065104 (2015).
44. P. Yan, R. Lin, S. Ruan, A. Liu, H. Chen, Y. Zheng, S. Chen, C. Guo, and J. Hu, Sci. Rep. **5**, 8690 (2015).
45. D. Mao, X. Cui, X. Gan, M. Li, W. Zhang, H. Lu, and J. Zhao, IEEE J. Sel. Top. Quantum Electron. **24**, 1100406 (2018).
46. W. Liu, L. Pang, H. Han, W. Tian, H. Chen, M. Lei, P. Yan, and Z. Wei, Sci. Rep. **6**, 19997 (2016).
47. Y. Ge, W. Huang, F. Yang, J. Liu, C. Wang, Y. Wang, J. Guo, F. Zhang, Y. Song, S. Xu, D. Fan, and H. Zhang, Nanoscale **11**, 6828 (2019).
48. X. Liu, D. Han, Z. Sun, C. Zeng, H. Lu, D. Mao, Y. Cui, and F. Wang, Sci. Rep. **3**, 2718 (2013).
49. X. Chen, Z. Deng, and J. Yao, IEEE Trans. Microwave Theory Tech. **54**, 804 (2006).
50. B. Lin, M. Jiang, S. C. Tjin, and P. Shum, IEEE Photon. Technol. Lett. **23**, 1292 (2011).
51. J.-R. Qian, J. Su, and L. Hong, Opt. Commun. **281**, 4432 (2008).
52. Y. Zhou, P. C. Chui, and K. K. Y. Wong, IEEE Photon. Technol. Lett. **25**, 385 (2013).
53. W. He, D. Li, L. Zhu, M. Dong, and F. Luo, IEEE Photon. J. **9**, 7202108 (2017).
54. G. Yin, S. Lou, X. Wang, and B. Han, Laser Phys. Lett. **10**, 125110 (2013).
55. J. Gutierrez-Gutierrez, R. Rojas-Laguna, J. M. Estudillo-Ayala, J. M. Sierra-Hernández, D. Jauregui-Vazquez, M. Vargas-Treviño, L. Tepech-Carrillo, and R. Grajales-Coutiño, Opt. Commun. **374**, 39 (2016).
56. J. M. Sierra-Hernandez, R. Rojas-Laguna, E. Vargas-Rodriguez, J. M. Estudillo-Ayala, D. Jauregui-Vazquez, A. D. Guzmán-Chávez, and P. Zaca-Moran, Laser Phys. **23**, 125103 (2013).
57. P. Zhang, T. Wang, W. Ma, K. Dong, and H. Jiang, Appl. Opt. **54**, 4667 (2015).
58. J. E. Antonio-Lopez, J. J. Sanchez-Mondragon, P. LiKamWa, and D. A. May-Arrioja, Laser Phys. **24**, 085108 (2014).
59. X. He, X. Fang, C. Liao, D. Wang, and J. Sun, Opt. Express **17**, 21773 (2009).
60. T. Sun, G. Kai, Z. Wang, C. Wang, C. Zhang, Y. Liu, J. Liu, W. Zhang, S. Yuan, X. J. M. Dong, and O. T. Letters, Opt. Technol. Lett. **46**, 162 (2005).
61. H. G. Pan, X. F. Yang, J. L. Yu, Z. R. Tong, and F. F. Wei, Appl. Mech. Mater. **130–134**, 4036 (2011).
62. X. M. Liu, Y. Chung, A. Lin, W. Zhao, K. Q. Lu, Y. S. Wang, and T. Y. Zhang, Laser Phys. Lett. **5**, 904 (2008).
63. F. Yang, D. N. Wang, Z. Wang, L. Li, C. L. Zhao, B. Xu, S. Jin, S. Y. Cao, and Z. J. Fang, Opt. Express **26**, 927 (2018).
64. J. Hernandez-Cordero, V. Kozlov, A. Carter, and T. Morse, IEEE Photon. Technol. Lett. **10**, 941 (1998).
65. J. Cheng, W. Chen, and G. Chen, Opt. Laser Technol. **78**, 71 (2016).
66. Y. Wang, Y. Zhou, S. Yan, Y. Tang, and J. Xu, IEEE Photon. Technol. Lett. **28**, 1193 (2016).
67. B. Guo, Y. Yao, Y.-F. Yang, Y.-J. Yuan, R.-L. Wang, S.-G. Wang, Z.-H. Ren, and B. Yan, J. Appl. Phys. **117**, 063108 (2015).
68. L. Y. Wook and L. Byoungho, IEEE Photon. Technol. Lett. **15**, 795 (2003).
69. X. Feng, Y. Liu, S. Fu, S. Yuan, and X. Dong, IEEE Photon. Technol. Lett. **16**, 762 (2004).
70. S. Yao, G. Ren, Y. Yang, Y. Shen, Y. Jiang, S. Xiao, and S. Jian, Laser Phys. Lett. **15**, 095001 (2018).
71. X. Feng, Y. Liu, S. Yuan, G. Kai, W. Zhang, and X. Dong, Opt. Express **12**, 3834 (2004).
72. X. Zhao, M. Dong, Y. Zhang, F. Luo, and L. Zhu, Opt. Laser Technol. **112**, 500 (2019).
73. X. Feng, H.-y. Tam, and P. Wai, Opt. Express **14**, 8205 (2006).
74. Z. Zhang, L. Zhan, K. Xu, J. Wu, Y. Xia, and J. Lin, Opt. Lett. **33**, 324 (2008).
75. W. Peng, F. Yan, Q. Li, S. Liu, T. Feng, and S. Tan, Laser Phys. Lett. **10**, 115102 (2013).

76. X. Feng, H.-Y. Tam, H. Liu, and P. K. A. Wai, Opt. Commun. **268**, 278 (2006).
77. K. Smith, N. Doran, and P. Wigley, Opt. Lett. **15**, 1294 (1990).
78. Z. Yan, X. Li, Y. Tang, P. P. Shum, X. Yu, Y. Zhang, and Q. J. Wang, Opt. Express **23**, 4369 (2015).
79. I. Duling, C.-J. Chen, P. Wai, and C. R. Menyuk, IEEE J. Quantum Electron. **30**, 194 (1994).
80. H. B. Sun, X. M. Liu, L. R. Wang, X. H. Li, and D. Mao, Laser Phys. **20**, 1994 (2010).
81. N. A. Cholan, M. H. Al-Mansoori, A. S. Noor, A. Ismail, and M. A. Mahdi, Opt. Express **21**, 6131 (2013).
82. D. Chen, B. Sun, and Y. Wei, Laser Phys. **20**, 1733 (2010).
83. S. W. Harun, R. Parvizi, S. Shahi, and H. Ahmad, Laser Phys. Lett. **6**, 813 (2009).
84. X. Yang, X. Dong, S. Zhang, F. Lu, X. Zhou, and C. Lu, IEEE Photon. Technol. Lett. **17**, 2538 (2005).
85. Y.-G. Han, T. V. A. Tran, and S. B. Lee, Opt. Lett. **31**, 697 (2006).
86. N. A. Awang, M. Z. Zulkifli, A. A. Latif, S. W. Harun, and H. Ahmad, J. Opt. **13**, 075401 (2011).
87. X. Liu, X. Yang, F. Lu, J. Ng, X. Zhou, and C. Lu, Opt. Express **13**, 142 (2005).
88. H. Young-Geun, K. Chang-Seok, J. U. Kang, P. Un-Chul, and Y. Chung, IEEE Photon. Technol. Lett. **15**, 383 (2003).
89. G. Mamdoohi, A. R. Sarmani, M. H. A. Bakar, and M. A. Mahdi, IEEE Photon. J. **10**, 7201011 (2018).
90. N. A. M. Ahmad Hambali, M. H. Al-Mansoori, M. Ajiya, A. A. A. Bakar, S. Hitam, and M. A. Mahdi, Laser Phys. **21**, 1656 (2011).
91. C. Ma, A. Khanolkar, and A. Chong, Opt. Lett. **44**, 1234 (2019).
92. C. Ma, X. Tian, B. Gao, and G. Wu, Opt. Commun. **410**, 941 (2018).
93. H. L. Chen, H. Zhang, H. W. Zhang, X. Zhao, Y. T. Xu, Y. G. Zou, X. H. Ma, and L. Jin, Appl. Opt. **57**, 7070 (2018).
94. J. Du, Q. Wang, G. Jiang, C. Xu, C. Zhao, Y. Xiang, Y. Chen, S. Wen, and H. Zhang, Sci. Rep. **4**, 6346 (2014).
95. J. Du, M. Zhang, Z. Guo, J. Chen, X. Zhu, G. Hu, P. Peng, Z. Zheng, and H. Zhang, Sci. Rep. **7**, 42357 (2017).
96. K. Wu, B. Chen, X. Zhang, S. Zhang, C. Guo, C. Li, P. Xiao, J. Wang, L. Zhou, W. Zou, and J. Chen, Opt. Commun. **406**, 214 (2018).
97. K. Tamura, E. Ippen, H. Haus, and L. Nelson, Opt. Lett. **18**, 1080 (1993).
98. H. Ahmad, S. A. Reduan, Z. A. Ali, M. A. Ismail, N. E. Ruslan, C. S. J. Lee, R. Puteh, and S. W. Harun, IEEE Photon. J. **8**, 1500107 (2016).
99. H. Ahmad, M. R. K. Soltanian, L. Narimani, I. S. Amiri, A. Khodaei, and S. W. Harun, IEEE Photon. J. **7**, 1502508 (2015).
100. Z. Kang, M. Liu, Z. Li, S. Li, Z. Jia, C. Liu, W. Qin, and G. Qin, Photon. Res. **6**, 549 (2018).
101. Y. Chen, J. Yin, H. Chen, J. Wang, P. Yan, and S. Ruan, IEEE Photon. J. **9**, 1501009 (2017).
102. W. Liu, M. Liu, M. Lei, S. Fang, and Z. Wei, IEEE J. Sel. Top. Quantum Electron. **24**, 0901005 (2018).
103. Y. Chen, G. Jiang, S. Chen, Z. Guo, X. Yu, C. Zhao, H. Zhang, Q. Bao, S. Wen, D. Tang, and D. Fan, Opt. Express **23**, 12823 (2015).
104. H. Li, F. Hu, Y. Tian, P. Wang, J. Zhang, and S. Xu, Opt. Express **27**, 14437 (2019).
105. M. Ma, W. Wen, Y. Zhang, C. Dou, J. Wang, L. Xie, C.-H. Ho, and Z. Wei, J. Mater. Chem. C **7**, 6900 (2019).
106. B. Bakhshi and P. A. Andrekson, IEEE Photon. Technol. Lett. **11**, 1387 (1999).
107. Y. Zhao and C. Shu, Appl. Phys. Lett. **72**, 1556 (1998).
108. G. Town, L. Chen, and P. Smith, IEEE Photon. Technol. Lett. **12**, 1459 (2000).
109. S. Li and K. T. Chan, Appl. Phys. Lett. **72**, 1954 (1998).
110. X. Wu, P. Huang, T. Huang, Z. Wu, Z. Cheng, B. Chen, K. Ren, and S. Fu, Laser Phys. Lett. **15**, 065103 (2018).
111. J. Bogusławski, Y. Wang, H. Xue, X. Yang, D. Mao, X. Gan, Z. Ren, J. Zhao, Q. Dai, G. Soboń, J. Sotor, and Z. Sun, Adv. Funct. Mater. **28**, 1801539 (2018).
112. A. F. J. Runge, N. G. R. Broderick, and M. Erkintalo, Optica **2**, 36 (2015).
113. M. Kues, C. Reimer, B. Wetzel, P. Roztocki, B. E. Little, S. T. Chu, T. Hansson, E. A. Viktorov, D. J. Moss, and R. Morandotti, Nat. Photon. **11**, 159 (2017).
114. R. Si Fodil, F. Amrani, C. Yang, A. Kellou, and P. Grelu, Phys. Rev. A **94**, 013813 (2016).
115. D. Li, H. Jussila, Y. Wang, G. Hu, T. Albrow-Owen, R. C. Howe, Z. Ren, J. Bai, T. Hasan, and Z. Sun, Sci. Rep. **8**, 2738 (2018).
116. P. Wu, Q. Zhou, Y. Wang, G. Deng, Y. Fan, S. Shen, Q. Xu, Y. Wang, H. Song, and Y. Wang, Appl. Opt. **58**, 5143 (2019).
117. H. Zhang, L. Jin, H. Zhang, Y. Xu, L. Shi, T. Wang, H. Chen, D. Wang, and X. Ma, Opt. Commun. **452**, 7 (2019).
118. H. Zhang, L. Jin, Y. Xu, H. Zhang, L. Shi, T. Wang, W. Pan, and X. Ma, Appl. Opt. **58**, 5788 (2019).
119. X. Zhu, C. Wang, G. Zhang, and R. Xu, Appl. Phys. B **118**, 69 (2014).
120. D. Y. Tang, L. M. Zhao, B. Zhao, and A. Q. Liu, Phys. Rev. A **72**, 043816 (2005).
121. A. Latiff, H. Shamsudin, Z. Tiu, H. Ahmad, and S. Harun, J. Nonlinear Opt. Phys. Mater. **25**, 1650034 (2016).
122. C. Song, W. Xu, Z. Luo, A. Luo, and W. Chen, Opt. Commun. **282**, 4408 (2009).
123. Z. C. Luo, A. P. Luo, and W. C. Xu, IEEE Photon. J. **3**, 64 (2011).
124. Z. Yan, Y. Tang, B. Sun, T. Liu, X. Li, P. S. Ping, X. Yu, Y. Zhang, and Q. J. Wang, Opt. Lett. **40**, 1916 (2015).
125. C. Guo, R. Luo, W. Liu, S. Ruan, J. Yang, P. Yan, J. Wang, and P. Hua, Opt. Commun. **406**, 107 (2018).
126. X. Jin, X. Wang, X. Wang, and P. Zhou, Appl. Opt. **54**, 8260 (2015).
127. N. Kuse, J. Jiang, C. C. Lee, T. R. Schibli, and M. E. Fermann, Opt. Express **24**, 3095 (2016).
128. J. Sun, Y. Zhou, Y. Dai, J. Li, F. Yin, J. Dai, and K. Xu, Appl. Opt. **57**, 1492 (2018).
129. P. Bowen, M. Erkintalo, and N. G. R. Broderick, Opt. Commun. **410**, 447 (2018).
130. M. Michalska and J. Swiderski, Opt. Laser Technol. **118**, 121 (2019).
131. M. Zhang, R. C. T. Howe, R. I. Woodward, E. J. R. Kelleher, F. Torrisi, G. Hu, S. V. Popov, J. R. Taylor, and T. Hasan, Nano Res. **8**, 1522 (2015).
132. S. Huang, Y. Wang, P. Yan, J. Zhao, H. Li, and R. Lin, Opt. Express **22**, 11417 (2014).
133. J. Zhao, Y. Wang, S. Ruan, P. Yan, H. Zhang, Y. H. Tsang, J. Yang, and G. Huang, J. Opt. Soc. Am. B **31**, 716 (2014).
134. A. K. Geim, Science **324**, 1530 (2009).
135. H. Zhang, ACS Nano **9**, 9451 (2015).
136. M. Zhang, Q. Wu, F. Zhang, L. Chen, X. Jin, Y. Hu, Z. Zheng, and H. Zhang, Adv. Opt. Mater. **7**, 1800224 (2019).
137. F. Zhang, K. Chen, X. Jiang, Y. Wang, Y. Ge, L. Wu, S. Xu, Q. Bao, and H. Zhang, J. Mater. Chem. C **6**, 8977 (2018).
138. Z. Xie, F. Zhang, Z. Liang, T. Fan, Z. Li, X. Jiang, H. Chen, J. Li, and H. Zhang, Photon. Res. **7**, 494 (2019).
139. L. Jin, X. Ma, H. Zhang, H. Zhang, H. Chen, and Y. Xu, Opt. Express **26**, 31244 (2018).

140. H. Liu, X.-W. Zheng, M. Liu, N. Zhao, A.-P. Luo, Z.-C. Luo, W.-C. Xu, H. Zhang, C.-J. Zhao, and S.-C. Wen, Opt. Express **22**, 6868 (2014).
141. M. A. Bandres, S. Wittek, G. Harari, M. Parto, J. Ren, M. Segev, D. N. Christodoulides, and M. Khajavikhan, Science **359**, eaar4005 (2018).
142. Y. Chen, M. Wu, P. Tang, S. Chen, J. Du, G. Jiang, Y. Li, C. Zhao, H. Zhang, and S. Wen, Laser Phys. Lett. **11**, 055101 (2014).
143. P. Yan, R. Lin, H. Chen, H. Zhang, A. Liu, H. Yang, and S. Ruan, IEEE Photon. Technol. Lett. **27**, 264 (2015).
144. Q. Wang, Y. Chen, L. Miao, G. Jiang, S. Chen, J. Liu, X. Fu, C. Zhao, and H. Zhang, Opt. Express **23**, 7681 (2015).
145. K. Watanabe, T. Taniguchi, and H. Kanda, Nat. Mater. **3**, 404 (2004).
146. G. Cassabois, P. Valvin, and B. Gil, Nat. Photon. **10**, 262 (2016).
147. S. Dai, Q. Ma, M. K. Liu, T. Andersen, Z. Fei, M. D. Goldflam, M. Wagner, K. Watanabe, T. Taniguchi, M. Thiemens, F. Keilmann, G. C. Janssen, S. E. Zhu, P. Jarillo-Herrero, M. M. Fogler, and D. N. Basov, Nat. Nanotechnol. **10**, 682 (2015).
148. S. M. Kim, A. Hsu, M. H. Park, S. H. Chae, S. J. Yun, J. S. Lee, D. H. Cho, W. Fang, C. Lee, T. Palacios, M. Dresselhaus, K. K. Kim, Y. H. Lee, and J. Kong, Nat. Commun. **6**, 8662 (2015).
149. B. Chen, X. Zhang, K. Wu, H. Wang, J. Wang, and J. Chen, Opt. Express **23**, 26723 (2015).
150. Y. Jiang, L. Miao, G. Jiang, Y. Chen, X. Qi, X. F. Jiang, H. Zhang, and S. Wen, Sci. Rep. **5**, 16372 (2015).
151. W. Liu, M. Liu, Y. OuYang, H. Hou, G. Ma, M. Lei, and Z. Wei, Nanotechnology **29**, 174002 (2018).
152. W. Liu, M. Liu, Y. OuYang, H. Hou, M. Lei, and Z. Wei, Nanotechnology **29**, 394002 (2018).
153. Z. Jiang, H. Chen, J. Li, J. Yin, J. Wang, and P. Yan, Appl. Phys. Express **10**, 122702 (2017).
154. S. B. Lu, L. L. Miao, Z. N. Guo, X. Qi, C. J. Zhao, H. Zhang, S. C. Wen, D. Y. Tang, and D. Y. Fan, Opt. Express **23**, 11183 (2015).
155. X. Jin, G. Hu, M. Zhang, Y. Hu, T. Albrow-Owen, R. C. T. Howe, T. C. Wu, Q. Wu, Z. Zheng, and T. Hasan, Opt. Express **26**, 12506 (2018).
156. M. H. M. Ahmed, A. A. Latiff, H. Arof, and S. W. Harun, Laser Phys. Lett. **13**, 095104 (2016).
157. C. Ma, X. Tian, B. Gao, and G. Wu, Opt. Commun. **406**, 177 (2018).
158. Z. C. Luo, M. Liu, Z. N. Guo, X. F. Jiang, A. P. Luo, C. J. Zhao, X. F. Yu, W. C. Xu, and H. Zhang, Opt. Express **23**, 20030 (2015).
159. C. Xing, G. Jing, X. Liang, M. Qiu, Z. Li, R. Cao, X. Li, D. Fan, and H. Zhang, Nanoscale **9**, 8096 (2017).
160. X. Ren, Z. Li, Z. Huang, D. Sang, H. Qiao, X. Qi, J. Li, J. Zhong, and H. Zhang, Adv. Funct. Mater. **27**, 1606834 (2017).
161. X. Ren, J. Zhou, X. Qi, Y. Liu, Z. Huang, Z. Li, Y. Ge, S. C. Dhanabalan, J. S. Ponraj, S. Wang, J. Zhong, and H. Zhang, Adv. Energy Mater. **7**, 1700396 (2017).
162. E. I. Ismail, N. A. Kadir, A. A. Latiff, H. Ahmad, and S. W. Harun, RSC Adv. **6**, 72692 (2016).
163. Y. Wang, F. Zhang, X. Tang, X. Chen, Y. Chen, W. Huang, Z. Liang, L. Wu, Y. Ge, Y. Song, J. Liu, D. Zhang, J. Li, and H. Zhang, Laser Photon. Rev. **12**, 1800016 (2018).
164. L. Lu, X. Tang, R. Cao, L. Wu, Z. Li, G. Jing, B. Dong, S. Lu, Y. Li, Y. Xiang, J. Li, D. Fan, and H. Zhang, Adv. Opt. Mater. **5**, 1700301 (2017).
165. Y. Wang, P. Huang, M. Ye, R. Quhe, Y. Pan, H. Zhang, H. Zhong, J. Shi, and J. Lu, Chem. Mater. **29**, 2191 (2017).
166. Y. Song, Z. Liang, X. Jiang, Y. Chen, Z. Li, L. Lu, Y. Ge, K. Wang, J. Zheng, S. Lu, J. Ji, and H. Zhang, 2D Mater. **4**, 045010 (2017).
167. Y. I. Jhon, J. Koo, B. Anasori, M. Seo, J. H. Lee, Y. Gogotsi, and Y. M. Jhon, Adv. Mater. **29**, 1702496 (2017).
168. J. He, F. Gao, Y.-L. Li, X.-F. Liu, H. Wu, Z.-Q. Jiang, and H.-K. Wu, J. Coord. Chem. **72**, 452 (2019).
169. Y. Dong, S. Chertopalov, K. Maleski, B. Anasori, L. Hu, S. Bhattacharya, A. M. Rao, Y. Gogotsi, V. N. Mochalin, and R. Podila, Adv. Mater. **30**, 1705714 (2018).
170. Y. Song, Y. Chen, X. Jiang, Y. Ge, Y. Wang, K. You, K. Wang, J. Zheng, J. Ji, Y. Zhang, J. Li, and H. Zhang, Adv. Opt. Mater. **7**, 1801777 (2019).
171. G. Gao, G. Ding, J. Li, K. Yao, M. Wu, and M. Qian, Nanoscale **8**, 8986 (2016).
172. G. Zhang, X. Zang, Z. Li, C. Wang, and Z. Wang, Talanta **129**, 600 (2014).
173. Z. Sun, X. Jiang, Q. Wen, W. Li, and H. Zhang, J. Mater. Chem. C **7**, 4662 (2019).
174. X. Jiang, L. Zhang, S. Liu, Y. Zhang, Z. He, W. Li, F. Zhang, Y. Shi, W. Lü, Y. Li, Q. Wen, J. Li, J. Feng, S. Ruan, Y.-J. Zeng, X. Zhu, Y. Lu, and H. Zhang, Adv. Opt. Mater. **6**, 1800561 (2018).
175. X. Chen, M. Addicoat, E. Jin, L. Zhai, H. Xu, N. Huang, Z. Guo, L. Liu, S. Irle, and D. Jiang, J. Am. Chem. Soc. **137**, 3241 (2015).
176. N. Huang, P. Wang, and D. Jiang, Nat. Rev. Mater. **1**, 16068 (2016).
177. A. Martinez and Z. Sun, Nat. Photon. **7**, 842 (2013).
178. Q. Wang, T. Chen, B. Zhang, M. Li, Y. Lu, and K. P. Chen, Appl. Phys. Lett. **102**, 131117 (2013).
179. A. Martinez, K. Fuse, B. Xu, and S. Yamashita, Opt. Express **18**, 23054 (2010).
180. P. Mouchel, G. Semaan, A. Niang, M. Salhi, M. Le Flohic, and F. Sanchez, Appl. Phys. Lett. **111**, 031106 (2017).
181. P. Yan, R. Lin, S. Ruan, A. Liu, and H. Chen, Opt. Express **23**, 154 (2015).
182. H. Zhang, D. Tang, X. Wu, and L. Zhao, Opt. Express **17**, 12692 (2009).
183. Y. Mashiko, E. Fujita, and M. Tokurakawa, Opt. Express **24**, 26515 (2016).
184. O. Okhotnikov, T. Jouhti, J. Konttinen, S. Karirinne, and M. Pessa, Opt. Lett. **28**, 364 (2003).
185. W. Yang, J. Hou, B. Zhang, R. Song, and Z. Liu, Appl. Opt. **51**, 5664 (2012).
186. J. Li, D. D. Hudson, Y. Liu, and S. D. Jackson, Opt. Lett. **37**, 3747 (2012).
187. B. Guo, Chin. Opt. Lett. **16**, 020004 (2018).
188. Z. Q. Luo, J. Z. Wang, M. Zhou, H. Y. Xu, Z. P. Cai, and C. C. Ye, Laser Phys. Lett. **9**, 229 (2012).
189. Z. Luo, Y. Huang, J. Wang, H. Cheng, Z. Cai, and C. Ye, IEEE Photon. Technol. Lett. **24**, 1539 (2012).
190. Z. Sun, T. Hasan, F. Torrisi, D. Popa, G. Privitera, F. Wang, F. Bonaccorso, D. M. Basko, and A. C. Ferrari, ACS Nano **4**, 803 (2010).
191. F. Bonaccorso, Z. Sun, T. Hasan, and A. C. Ferrari, Nat. Photon. **4**, 611 (2010).
192. Y.-W. Song, S.-Y. Jang, W.-S. Han, and M.-K. Bae, Appl. Phys. Lett. **96**, 051122 (2010).
193. H. Zhang, D. Y. Tang, L. M. Zhao, Q. L. Bao, K. P. Loh, B. Lin, and S. C. Tjin, Laser Phys. Lett. **7**, 591 (2010).
194. D. Popa, Z. Sun, T. Hasan, F. Torrisi, F. Wang, and A. C. Ferrari, Appl. Phys. Lett. **98**, 073106 (2011).

195. Q. Bao, H. Zhang, Z. Ni, Y. Wang, L. Polavarapu, Z. Shen, Q.-H. Xu, D. Tang, and K. P. Loh, Nano Res. **4**, 297 (2010).
196. N. Zhao, M. Liu, H. Liu, X. W. Zheng, Q. Y. Ning, A. P. Luo, Z. C. Luo, and W. C. Xu, Opt. Express **22**, 10906 (2014).
197. J. Sotor, G. Sobon, J. Tarka, I. Pasternak, A. Krajewska, W. Strupinski, and K. M. Abramski, Opt. Express **22**, 5536 (2014).
198. E. Hendry, P. J. Hale, J. Moger, A. K. Savchenko, and S. A. Mikhailov, Phys. Rev. Lett. **105**, 097401 (2010).
199. Z. Luo, M. Zhou, D. Wu, C. Ye, J. Weng, J. Dong, H. Xu, Z. Cai, and L. Chen, J. Lightwave Technol. **29**, 2732 (2011).
200. Z. Wang, C. Li, J. Ye, Z. Wang, and Y.-G. Liu, Laser Phys. Lett. **16**, 025103 (2019).
201. G. Sobon, Photon. Res. **3**, A56 (2015).
202. C. Chi, J. Lee, J. Koo, and J. H. Lee, Laser Phys. **24**, 105106 (2014).
203. J. Lee, J. Koo, and J. H. Lee, Opt. Eng. **55**, 081309 (2016).
204. C. Zhao, Y. Zou, Y. Chen, Z. Wang, S. Lu, H. Zhang, S. Wen, and D. Tang, Opt. Express **20**, 27888 (2012).
205. Z. Dou, Y. Song, J. Tian, J. Liu, Z. Yu, and X. Fang, Opt. Express **22**, 24055 (2014).
206. Y.-H. Lin, C.-Y. Yang, S.-F. Lin, W.-H. Tseng, Q. Bao, C.-I. Wu, and G.-R. Lin, Laser Phys. Lett. **11**, 055107 (2014).
207. Y.-H. Lin, S.-F. Lin, Y.-C. Chi, C.-L. Wu, C.-H. Cheng, W.-H. Tseng, J.-H. He, C.-I. Wu, C.-K. Lee, and G.-R. Lin, ACS Photon. **2**, 481 (2015).
208. J. Boguslawski, G. Sobon, R. Zybala, and J. Sotor, Opt. Lett. **40**, 2786 (2015).
209. J. Boguslawski, J. Sotor, G. Sobon, J. Tarka, J. Jagiello, W. Macherzynski, L. Lipinska, and K. M. Abramski, Laser Phys. **24**, 105111 (2014).
210. S. Chen, C. Zhao, Y. Li, H. Huang, S. Lu, H. Zhang, and S. Wen, Opt. Mater. Express **4**, 587 (2014).
211. S. Lu, C. Zhao, Y. Zou, S. Chen, Y. Chen, Y. Li, H. Zhang, S. Wen, and D. Tang, Opt. Express **21**, 2072 (2013).
212. B. Guo and Y. Yao, Opt. Eng. **55**, 081315 (2016).
213. Z. Wang, R. He, Y.-g. Liu, H. Zhang, S. Han, H. Li, G. Wang, G. Yang, and Z. Wang, Appl. Phys. Express **11**, 072504 (2018).
214. J. Wang, W. Lu, J. Li, H. Chen, Z. Jiang, J. Wang, W. Zhang, M. Zhang, I. Ling Li, Z. Xu, W. Liu, and P. Yan, IEEE J. Sel. Top. Quantum Electron. **24**, 1100706 (2018).
215. J. Lee, J. Park, J. Koo, Y. M. Jhon, and J. H. Lee, J. Opt. **18**, 035502 (2016).
216. L. Li, Y. Su, Y. Wang, X. Wang, Y. Wang, X. Li, D. Mao, and J. Si, IEEE J. Sel. Top. Quantum Electron. **23**, 44 (2017).
217. M. Liu, A. Luo, W. Xu, and Z. Luo, Chin. Opt. Lett. **16**, 020008 (2018).
218. P. Yan, H. Chen, J. Yin, Z. Xu, J. Li, Z. Jiang, W. Zhang, J. Wang, I. L. Li, Z. Sun, and S. Ruan, Nanoscale **9**, 1871 (2017).
219. Z. Luo, Y. Li, M. Zhong, Y. Huang, X. Wan, J. Peng, and J. Weng, Photon. Res. **3**, A79 (2015).
220. R. Woodward and E. Kelleher, Appl. Sci. **5**, 1440 (2015).
221. K. Wu, X. Zhang, J. Wang, X. Li, and J. Chen, Opt. Express **23**, 11453 (2015).
222. B. Guo, S. Li, Y.-x. Fan, and P. Wang, Opt. Commun. **406**, 66 (2018).
223. K. Wang, J. Wang, J. Fan, M. Lotya, A. O'Neill, D. Fox, Y. Feng, X. Zhang, B. Jiang, Q. Zhao, H. Zhang, J. N. Coleman, L. Zhang, and W. J. Blau, ACS Nano. **7**, 9260 (2013).
224. B. Guo, Y. Yao, P.-G. Yan, K. Xu, J.-J. Liu, S.-G. Wang, and Y. Li, IEEE Photon. Technol. Lett. **28**, 323 (2016).
225. J. Sotor, G. Sobon, W. Macherzynski, P. Paletko, and K. M. Abramski, Appl. Phys. Lett. **107**, 051108 (2015).
226. K. Park, J. Lee, Y. T. Lee, W.-K. Choi, J. H. Lee, and Y.-W. Song, Annalen der Physik. **527**, 770 (2015).
227. J. Liu, Y. Chen, Y. Li, H. Zhang, S. Zheng, and S. Xu, Photon. Res. **6**, 198 (2018).
228. Y. Xu, W. Wang, Y. Ge, H. Guo, X. Zhang, S. Chen, Y. Deng, Z. Lu, and H. Zhang, Adv. Funct. Mater. **27**, 1702437 (2017).
229. R. Zhao, J. He, X. Su, Y. Wang, X. Sun, H. Nie, B. Zhang, and K. Yang, IEEE J. Sel. Top. Quantum Electron. **24**, 0900405 (2018).
230. M. B. Hisyam, M. F. M. Rusdi, A. A. Latiff, and S. W. Harun, IEEE J. Sel. Top. Quantum Electron. **23**, 39 (2017).
231. Z. Qin, G. Xie, H. Zhang, C. Zhao, P. Yuan, S. Wen, and L. Qian, Opt. Express **23**, 24713 (2015).
232. J. Li, H. Luo, B. Zhai, R. Lu, Z. Guo, H. Zhang, and Y. Liu, Sci. Rep. **6**, 30361 (2016).
233. R. Zhao, J. Li, B. Zhang, X. Li, X. Su, Y. Wang, F. Lou, H. Zhang, and J. He, Appl. Phys. Express **9**, 092701 (2016).
234. L. Yun, Opt. Express **25**, 32380 (2017).
235. B. Guo, Y. Yao, J.-J. Tian, Y.-F. Zhao, S. Liu, M. Li, and M.-R. Quan, IEEE Photon. Technol. Lett. **27**, 701 (2015).
236. Y. Cui, F. Lu, and X. Liu, Sci. Rep. **6**, 30524 (2016).
237. Y. Cui and X. Liu, Opt. Express **21**, 18969 (2013).
238. Y. D. Cui, X. M. Liu, and C. Zeng, Laser Phys. Lett. **11**, 055106 (2014).
239. J. Li, Y. Wang, H. Luo, Y. Liu, Z. Yan, Z. Sun, and L. Zhang, Photon. Res. **7**, 103 (2019).
240. X. Han, Appl. Opt. **57**, 807 (2018).
241. Z. Zhang, D. Popa, V. J. Wittwer, S. Milana, T. Hasan, Z. Jiang, A. C. Ferrari, and F. Ö. Ilday, Appl. Phys. Lett. **107**, 241107 (2015).
242. W. He, M. Pang, C. R. Menyuk, and P. St. J. Russell, Optica **3**, 1366 (2016).
243. L. Hou, H. Guo, Y. Wang, J. Sun, Q. Lin, Y. Bai, and J. Bai, Opt. Express **26**, 9063 (2018).
244. Z. Wang, L. Zhan, X. Fang, C. Gao, and K. Qian, J. Lightwave Technol. **34**, 4128 (2016).
245. V. Lazarev, A. Krylov, D. Dvoretskiy, S. Sazonkin, A. Pnev, S. Leonov, D. Shelestov, M. Tarabrin, V. Karasik, A. Kireev, and M. Gubin, IEEE Trans. Ultrason. Ferroelectr. Freq. Control. **63**, 1028 (2016).
246. B. Oktem, C. Ülgüdür, and F. Ö. Ilday, Nat. Photon. **4**, 307 (2010).
247. Z. Wang, L. Zhan, X. Fang, and H. Luo, J. Opt. Soc. Am. B **34**, 2325 (2017).
248. M. Olivier and M. Piche, Opt. Express **24**, 2336 (2016).
249. P. Grelu and N. Akhmediev, Nat. Photon. **6**, 84 (2012).
250. B. Liu, L. Gao, W. W. Cheng, X. S. Tang, C. Gao, Y. L. Cao, Y. J. Li, and T. Zhu, Opt. Express **26**, 7155 (2018).
251. T. Du, Z. Luo, R. Yang, Y. Huang, Q. Ruan, Z. Cai, and H. Xu, Opt. Lett. **42**, 462 (2017).
252. H. Zhang, D. Y. Tang, L. M. Zhao, and X. Wu, Phys. Rev. A **80**, 045803 (2009).
253. Y. F. Song, J. Guo, L. M. Zhao, D. Y. Shen, and D. Y. Tang, Opt. Lett. **39**, 3484 (2014).
254. H. H. Liu and K. K. Chow, Opt. Express **22**, 29708 (2014).
255. W. Liu, L. Pang, H. Han, Z. Shen, M. Lei, H. Teng, and Z. Wei, Photon. Res. **4**, 111 (2016).
256. Q.-Y. Ning, S.-K. Wang, A.-P. Luo, Z.-B. Lin, Z.-C. Luo, and W.-C. Xu, IEEE Photon. J. **4**, 1647 (2012).
257. M. Zhang, E. Kelleher, A. Pozharov, E. Obraztsova, S. Popov, and J. Taylor, Opt. Lett. **36**, 3984 (2011).
258. M. Rusu, R. Herda, and O. G. Okhotnikov, Opt. Lett. **29**, 2246 (2004).
259. C. Jia, B. J. Shastri, N. Abdukerim, M. Rochette, P. R. Prucnal, M. Saad, and L. R. Chen, Sci. Rep. **6**, 36071 (2016).
260. C. Guo, W. Liu, S. Ruan, J. Yu, Y. Chen, P. Yan, J. Wang, S. Jain, and P. Hua, IEEE Photon. J. **9**, 1502609 (2017).

261. J. Li, H. Luo, L. Wang, Y. Liu, Z. Yan, K. Zhou, L. Zhang, and S. K. Turistsyn, Sci. Rep. **5**, 10770 (2015).
262. J. Li, Z. Zhang, L. Du, L. Miao, J. Yi, B. Huang, Y. Zou, C. Zhao, and S. Wen, Photon. Res. **7**, 260 (2019).
263. X. Jiang, S. Liu, W. Liang, S. Luo, Z. He, Y. Ge, H. Wang, R. Cao, F. Zhang, Q. Wen, J. Li, Q. Bao, D. Fan, and H. Zhang, Laser Photon. Rev. **12**, 1700229 (2018).
264. R. Li, L. Zhang, L. Shi, and P. Wang, ACS Nano **11**, 3752 (2017).
265. Y. Yao, Z. Lin, Z. Li, X. Song, K.-S. Moon, and C.-P. Wong, J. Mater. Chem. **22**, 13494 (2012).
266. K. R. Paton, E. Varrla, C. Backes, R. J. Smith, U. Khan, A. O'Neill, C. Boland, M. Lotya, O. M. Istrate, P. King, T. Higgins, S. Barwich, P. May, P. Puczkarski, I. Ahmed, M. Moebius, H. Pettersson, E. Long, J. Coelho, S. E. O'Brien, E. K. McGuire, B. M. Sanchez, G. S. Duesberg, N. McEvoy, T. J. Pennycook, C. Downing, A. Crossley, V. Nicolosi, and J. N. Coleman, Nat. Mater. **13**, 624 (2014).
267. E. Varrla, C. Backes, K. R. Paton, A. Harvey, Z. Gholamvand, J. McCauley, and J. N. Coleman, Chem. Mater. **27**, 1129 (2015).
268. Y. Huang, E. Sutter, N. N. Shi, J. Zheng, T. Yang, D. Englund, H.-J. Gao, and P. Sutter, ACS Nano **9**, 10612 (2015).
269. X. Zhao, Z. Zheng, L. Liu, Y. Liu, Y. Jiang, X. Yang, and J. Zhu, Opt. Express **19**, 1168 (2011).
270. S. D. Jackson, Nat. Photon. **6**, 423 (2012).
271. S. Tokita, M. Murakami, S. Shimizu, M. Hashida, and S. Sakabe, Opt. Lett. **34**, 3062 (2009).
272. A. Schliesser, N. Picqué, and T. W. Hänsch, Nat. Photon. **6**, 440 (2012).
273. C. R. Petersen, U. Møller, I. Kubat, B. Zhou, S. Dupont, J. Ramsay, T. Benson, S. Sujecki, N. Abdel-Moneim, Z. Tang, D. Furniss, A. Seddon, and O. Bang, Nat. Photon. **8**, 830 (2014).
274. C. Xia, M. Kumar, O. P. Kulkarni, M. N. Islam, F. L. Terry Jr, M. J. Freeman, M. Poulain, and G. Mazé, Opt. Lett. **31**, 2553 (2006).
275. M. R. Majewski, R. I. Woodward, and S. D. Jackson, Opt. Lett. **44**, 1698 (2019).
276. G. Zhu, X. Zhu, K. Balakrishnan, R. A. Norwood, and N. Peyghambarian, Opt. Mater. Express **3**, 1365 (2013).
277. C. Wei, X. Zhu, F. Wang, Y. Xu, K. Balakrishnan, F. Song, R. A. Norwood, and N. Peyghambarian, Opt. Lett. **38**, 3233 (2013).
278. J. Li, H. Luo, L. Wang, C. Zhao, H. Zhang, H. Li, and Y. Liu, Opt. Lett. **40**, 3659 (2015).
279. S. Wang, Y. Tang, J. Yang, H. Zhong, and D. Fan, Laser Phys. **29**, 025101 (2019).
280. A. Martinez and S. Yamashita, Appl. Phys. Lett. **101**, 041118 (2012).
281. M. N. Sysak, J. O. Anthes, J. E. Bowers, O. Raday, and R. Jones, Opt. Express **16**, 12478 (2008).
282. T. Ohyama, Y. Doi, W. Kobayashi, S. Kanazawa, K. Takahata, A. Kanda, T. Kurosaki, T. Tanaka, T. Ohno, H. Sanjoh, and T. Hashimoto, J. Lightwave Technol. **34**, 1038 (2016).
283. R. I. Woodward and E. J. Kelleher, Sci. Rep. **6**, 37616 (2016).
284. U. Andral, R. S. Fodil, F. Amrani, F. Billard, E. Hertz, and P. Grelu, Optica **2**, 275 (2015).
285. G. Pu, L. Yi, L. Zhang, and W. Hu, Optica **6**, 362 (2019).
286. S. L. Brunton, F. Xing, and J. N. Kutz, IEEE J. Sel. Top. Quantum Electron. **20**, 464 (2014).